Microchim Acta (2017) 184:3069–3092
DOI 10.1007/s00604-017-2418-6

REVIEW ARTICLE

Gold nanorod-based electrochemical sensing of small biomolecules: A review

Mani Alagiri[1] · **Perumal Rameshkumar**[2] · **Alagarsamy Pandikumar**[3]

Received: 20 February 2017 / Accepted: 10 July 2017 / Published online: 22 July 2017

Abstract Gold nanorods (AuNRs) show high potential in electrochemical sensing owing to their excellent conductivity, electrocatalytic activity, selectivity and sensitivity. This review (with 99 refs.) summarizes the performance of AuNR-based electrochemical sensors based on the use of advanced nanocomposites. Following an introduction into the fields of biosensors and nanomaterials, the article summarizes the advantages and limitations of conventional analytical methods. A third section overviews the methods for preparation and characterization of AuNRs and nanocomposites including bimetallic nanorods, gold-metal oxide, gold-carbon nanotubes, gold-polymer, gold-graphene, gold-CNT and gold-enzymes conjugates. Their electrochemistry is treated next, with aspects related to the effects of rod size and shape, of thiol coatings on voltammetric signals, and on the behavior of 1-D AuNRs and respective arrays. Section 5 gives examples for non-enzymatic sensors for simple biomolecules, with subsections on sensors for hydrogen peroxide, nitric oxide, glucose, dopamine, NAD/NADH, cysteine, and some drugs. Section 6 covers enzyme-based sensors, with examples on sensors using peroxidases, oxidases and the like. The next sections cover DNA biosensors (such as for DNA biomarkers) and immunosensors, mainly for tumor markers. Possibilities for improving sensor performance are presented at the end of the review.

Keywords Selectivity · Immunosensor · Cyclic voltammetry · Glucose sensor · Hydrogen peroxide · Nitric oxide · Dopamine · DNA biosensors · Immunosensors · Electrochemical impedance spectroscopy · Linear sweep voltammetry · Chronoamperometry

Introduction

Biosensors usually are categorized as DNA biosensors, immunological biosensors, and enzyme-based biosensors, to mention the most common ones. Alternatively, they may be classified according to the type of transducer, examples being piezoelectrical, optical, electrochemical and thermal/calorimetric biosensors [1]. Among these sensors, electrochemical biosensors have received greater attention because of their high signal-to-noise ratio, relative simplicity, high sensitivity, rapid response and real time monitoring and they have shown potential importance in the field of biomedical .applications. In electrochemical biosensor, the transducer converts biological response into an electrical output signal. Potentiometry and amperometry are the two most commonly used measurements in electrochemical sensing application. In potentiometry, the analytical information observed by bio-recognition process is transformed into potential signal, whereas in amperometry, constant potential linked with reduction or oxidation of an electroactive species is examined and its output signals are into current [2, 3].

Various nanomaterials can be used to design and construct the electrochemical sensor including silicon, carbon nanotubes, conducting polymers, metals and metal oxides,

✉ Alagarsamy Pandikumar
pandikumarinbox@gmail.com

[1] Department of Physics and Nanotechnology, SRM University, SRM Nagar, Kattankulathur -603 203, India

[2] Department of Chemistry, Kalasalingam University (Kalasalingam Academy of Research and Education), Krishnankoil 626 126, India

[3] Electrochemical Materials Science and Functional Materials Division, CSIR-Central Electrochemical Research Institute, Karaikudi -630003, India

nanocantilivers, quantum dots, semiconductors and magnetic particles. These nanostructures offer a variety of biomolecules to be determined with high specificity and sensitivity [2, 3]. In particular, gold (Au) nanostructures have attracted considerable attention for electrochemical sensing of biomolecules because of their electronic, optical, and catalytic properties [4]. Gold nanocrystals present a large number of active surface sites with high curvatures. These surface sites have more dangling bonds, which considerably enhances the chemical reactivities and surface bonding characters of gold nanocrystal [4–8]. The morphology of gold nanocrystals is also a significant factor in governing their physical and chemical properties. A nonspherical gold nanocrystal shows anisotropic optical and electronic responses compared to spherical one that are measured by their topological aspects [9]. Among the different gold nanocrystals with nonspherical morphology, gold nanorods have received great attention due to their high surface area with efficient mass transport characteristics and favourable biocompatibility, which results in improved sensitivity and selectivity of the electrochemical sensors [5]. Table 1 summarizes the comparison of some of the typical features of AuNRs and AuNPs. The synthesis and characterization of gold nanorods have met an improvement in research activities since their first discovery in 1991 [6, 13–15]. This review is devoted to electrochemical biosensors with the use of gold nanorods to improve both of electrical conductivity and signal amplification for sensitive detection of small biomolecules such as hydrogen peroxide, nitric oxide, glucose, dopamine and its congeners and metabolites, NAD+ and NADH, L-cysteine, and complex biosensors such as DNA, enzymatic biosensors, and immunosensors.

Conventional detection methods: Advantages and limitations

In recent years, numerous analytical and spectroscopic methods including high-performance liquid chromatography (HPLC) [16], spectrophotometry [17], capillary electrophoresis (CE) [18], gas chromatography (GC) [19] and colorimetric analysis [20] have been developed for sensitive detection of biomolecules. Even though these methods show good analytical performance, the use of these methods requires sophisticated instrumentation, longer time, high-cost and also needs a skilled operator to carry out the experiments [21]. For example, GC is an analytical method which is used for the separation of volatile substance from a given mixture of compounds which are very difficult to separate and analyze. Colorimetric analysis is not possible for nanomaterials having absorption features only at UV wavelength region. Hence, the development of a simple method for the sensitive, rapid, and highly selective detection of biomolecules is an important task. In recent times, the improvements in electrochemical sensors have attracted greater attention owing to their advantages of simplicity, rapid response, easy operation, cost effectiveness, high sensitivity, excellent selectivity, capacity for real-time in situ detection and user friendly. An electrochemical sensor is able to generate an electrical output signal into the digital signal. Essentially, the response achieved in electrochemical sensors is owing to the interaction between chemistry and electricity which are based on amperometric, potentiometric and conductivity analysis. In the fabrication of chemically modified electrochemical biosensors, the detection of simple molecules takes into consideration of two main features; the development in electrocatalytic activity and the selectivity of simple biomolecules with several potential interfering species [22, 23].

Preparation and characterization of AuNRs

AuNRs were actively prepared by various techniques such as electrochemical synthesis, seed-mediated synthesis, template method, lithographic methods, and catalytic methods. Table 2 shows the summary of various synthetic methods, reagents and mechanism for the formation of AuNRs. Some syntheses and applications are shown in Fig. 1. The preparation process of the above mentioned techniques are as follows. The first report on the synthesis of high quality AuNRs was published

Table 1 Comparison of some of the characteristic features of AuNRs and AuNPs

Nanomaterial	Size range (nm)	Aspect ratio range	Absorption Wavelength range (λ_{max}, nm)	Color of colloidal solution	Ref.
AuNPs	(8.4 ± 1.0)- (180.5 ± 10.7)	-	518–720	wine red (size, ~10 nm)	[10]
AuNRs (high aspect ratio)	-	21–23 (Average ratio)	510–520 (transverse plasmon) 1300–2500 (longitudinal plasmon)	brown	[11]
AuNRs (low aspect ratio)	-	(2.7 ± 0.4)-(4.7 ± 0.7)	511–514 (transverse plasmon) 726–829 (longitudinal plasmon)	black (aspect ratio, 2.7 ± 0.4)	[12]

Table 2 Summary of various synthetic methods, reagents and mechanism for the formation of AuNRs

S.No	Synthetic Method	Reagents	Growth mechanism	Aspect ratio	Ref.
1	Electrolysis	Gold metal plate, Platinum metal plate, CTAB	Electrochemical oxidation/reduction process	~ 5	[24]
2	Surfactant template method	$HAuCl_4$, CTAB, $NaBH_4$, $AgNO_3$, Ascorbic acid	Seed mediated growth process	1	[27]
3	Size controlled seed growth	$HAuCl_4$, CTAB, $NaBH_4$, $AgNO_3$, Ascorbic acid, Glucose, Sodium citrate	Seed mediated growth & Ageing process	9, 16, 20, 21	[14]
4	Sulfide-arrested growth	$HAuCl_4$, CTAB, $NaBH_4$, $AgNO_3$, Ascorbic acid, Na_2S	Seed mediated growth process	3	[28]
5	Template mediated method	Porous alumina, Cu_2SO_4, $KAuCN_2$, Poly(vinylpyrrolidone)	Electrodeposition & Etching process	6, 8, 10, 12	[30]
6	Surfactant assisted growth	APTMS, $HAuCl_4$, CTAB, $NaBH_4$, $AgNO_3$, Ascorbic acid, mica sheet	Seed mediated growth process	NA	[33]
7	Surfactant assisted growth	MPTMS, $HAuCl_4$, CTAB, $NaBH_4$, $AgNO_3$, Ascorbic acid, mica sheet	Seed mediated growth process	6–12	[34]
8	Seeded substrate method	MPTMS, $HAuCl_4$, CTAB, $NaBH_4$, $AgNO_3$, Ascorbic acid, cetylpyridinium chloride, N-doped silica wafer	Seed mediated growth process	NA	[35]
9	Nanopatterning	MPTMS, $HAuCl_4$, CTAB, $NaBH_4$, $AgNO_3$, Ascorbic acid, Poly(dimethylsiloxane) 184 silicone elastomer base, 184 silicone elastomer curing agent,. Si/SiOx substrate	Seed mediated growth & Stamping process	NA	[37]

by Wang and co-workers through electrochemical method [24, 25]. In this process, gold metal and platinum metal plates served as an anode and cathode electrodes, respectively. Gold ions were generated in the form of $AuBr_4^-$ from gold metal anode through electrolysis process, which formed complexes with the cetyltrimethylammonium bromide (CTAB) micelle and then migrated to the cathode whereas gold ions were converted to gold atoms [6]. The presence of Ag metal plate which was theorized to generate Ag ions in solution, resulted in enhanced rod yield and length. AuNRs were prepared through the electrochemical synthesis with aspect ratios from 1 to 7 with a resultant longitudinal plasmon as high as 1050 nm with diameter of about 10 nm [26]. In 2001, Jana et al. [27] reported a concept of seed-mediated chemical growth; in this process colloidal AuNRs were prepared by the addition of citrate-capped small gold nanospheres, named

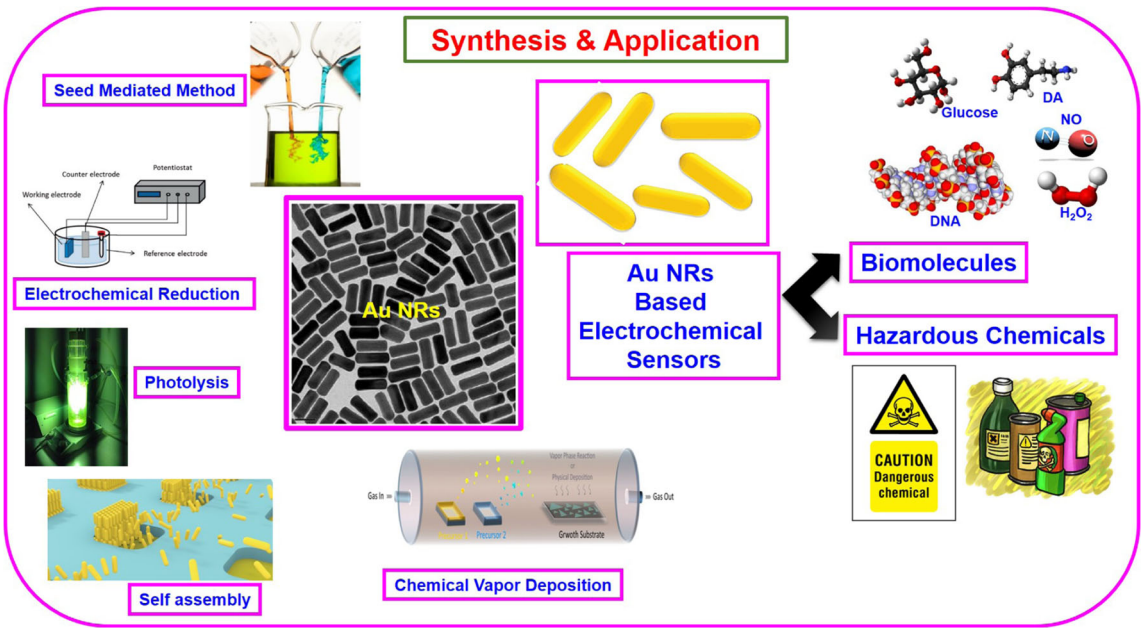

Fig. 1 Pictorial representation of gold nanorods synthesis and biosensor applications

as seed solution, to a bulk $HAuCl_2$ growth solution prepared by the reduction of $HAuCl_4$ with ascorbic acid in the presence of Ag ions and CTAB surfactant. In 2003, Nikoobakht and El-Sayed [14] reported two modifications to this synthesis method: replacing sodium citrate with a stronger CTAB stabilizer in the seed formation method and the aspect ratio of AuNRs was controlled by employing Ag ions. This procedure comprised of two steps: i) the seed solution were prepared via the reduction of auric acid in the presence of CTAB with ice-cold sodium borohydride and ii) the seed solution was added to the Au^+ stock solution in the presence of CTAB which is prepared via the reduction of $HAuCl_4$ with ascorbic acid. To facilitate the rod formation, silver nitrate was introduced to the gold solution before seed addition and to adjust the aspect ratio as well. This method gives rise to a high yield AuNRs (99%) with aspect ratios from 1.5 to 4.5 and shuns cyclic centrifugations for sphere separation [6, 28].

In template method, an anodized alumina membrane or nanoporous track-etched polycarbonate served as the template where gold atoms were deposited by gold ion precursor in an electrochemical cell through electrochemical reduction technique [29, 30]. Well-ordered arrangements of AuNRs with the long axis normal to the substrate were derived from the subsequent chemical etching of the template membrane. The pore diameter of the membrane template can control the width of the nanorods. Pore size of 5–200 nm can be synthesized in an acidic solution by the anodization of the aluminium metal [6]. Electron-beam lithography (EBL) is one of the most commonly used techniques for this purpose. The fabrication protocol starts through coating a substrate using an electron-sensitive resist that, when exposing to an electron beam, polymer was dissociated into smaller segments that can be particularly removed by washing with a developing agent. Thus, gold can be deposited by the patterns is written with an electron beam, which allow for the formation of nanometer-scale openings in the resist. The leftover unexposed resist and the gold deposited on it are simply removed by washing with acetone. Focused ion beam (FIB) lithography as an alternate top-down approach for the preparation of gold nanostructures, this process use a rastered ion beam, commonly gallium, to sputter away unwanted parts of a continuous film removing behind gold nanostructures of the preferred shape [6]. AuNRs were prepared by using both EBL and FIB methods [31, 32].

A catalytic synthesis procedure involves the use of catalytic seed nanospheres to directly grow 1D AuNRs on the substrates. Such a process is a well-established technique for fabricating substrate-based semiconductor nanowires. Taub et al., [33] reported, in order to facilitate nanoparticle attachment to the surface, the substrate was initially treated with a linker. Once attached, about 15% of the nanoparticles were able to produce nanorod growth when the substrate was kept in the aqueous solution. The leftover nanoparticles ascented a myriad of shapes including those that is hexagonal, triangular and spherical. Subsequent literature explains alternate means of linking the nanoparticles to the surface [34, 35] and the HgTe nanoparticles served as the seed-material [36]. Further, mieszawska et al. [37] have reported this method by using a microcontact printing technique to attach the gold nanoparticles to the substrate's surface by a stamp fabricated from a micrometer-scale patterns etched silicon wafer. During stamping, only the raised parts of the stamp come into contact with the substrate, nanorod growth can be supported by only site-specific areas, while the substrate remained bare. One can remove a considerable percentage of the oddly shaped nanostructures using adhesive tape by taking benefit of the fact that they have bad adhesion to the substrate [6].

Electrochemistry of AuNRs

One very exciting and important potential application of 1-D AuNRs is in the field of electrochemistry. The nanoelectrodes offer great opportunities to do electrochemistry in highly sensitive and to examine the kinetics of redox procedures that are too fast to assess at conventional macroscopic electrodes [38, 39]. Mariana Chirea et al. reported [40] size-dependent electrochemical properties. The authors have performed the electrochemical measurements for $n = 0$ represents to the bare Au, $n = 1$ to the 1,6HDT self-assembled monolayer (SAM), $n = 2a$ to the 1,6 hexanedithiol (1,6HDT)-$AuNR_1$ (37.5 nm in length and 17 nm in width, 2.20 aspect ratio) bilayer, $n = 2b$ to the 1,6HDT-$AuNR_2$ (48.0 nm in length and 17.14 nm in width, 2.80 aspect ratio) bilayer, and $n = 2c$ to the 1,6HDT-$AuNR_3$ (and 51 nm in length and 13.5 nm in width, 3.77 aspect ratio) bilayer. Figure 6 depicts the cyclic and square-wave voltammograms calculated at the bare Au electrode, Au-1,6HDT-SAM and Au-1,6HDT-AuNR-modified electrodes by 0.0005 M $[Fe(CN)_6]^{3-/4-}$ as redox probes and 0.1 M $NaClO_4$ as the supporting electrolyte. Compared to the type of thiol, the mercaptosuccinic acid (MSA) served as a first layer for the fabrication of multilayers consisted of polymers and spherical nanoparticles [37, 40]. The 1,6 HDT monolayer produced a pinhole-free film on the pure gold electrode. From the CV and SQWV performance of the Au-1,6HDT-SAM electrode ($n = 1$), author reported that within the applied potential window the 1,6HDT-SAM hindered the electron transfer between the metal surface and the redox species in solution. This was confirmed by the vanishing of the faradaic current at the Au-1,6HDT-SAM electrode ($n = 1$) as compared to that of the pure Au ($n = 0$), proving a dense packing of the 1,6HDT molecules on the gold electrode surface and accordingly the electronic communication blocked between $[Fe(CN)_6]^{3-/4-}$ in solution and the underlying gold electrode surface. The passivating effect is owing to the longer aliphatic chain of the 1,6HDT (C_6) as compared with that of MSA (C_2) [40–42].

Chirea et al. reported [43] density-dependent electrochemical properties of vertically aligned AuNRs. The electrochemical behavior of Au-1,6HDT-$AuNR_1$ (average length per width of 38.20 nm per 16.40 nm, 2.33 aspect ratio) and Au-1,6HDT-$AuNR_2$ (average length per width of 50 nm per 15.82 nm, 3.16 aspect ratio) modified electrodes as a function of the adsorption time of the AuNRs were measured through cyclic voltammetry (CV), square wave voltammetry (SWV), and electrochemical impedance spectroscopy. For these experiments, $n = 0$ represents to the pure gold electrode, $n = 1$ represents to the Au-1,6HDTSAM modified electrode, and $n = 2a_1$, $2a_2$, $2a_3$, and $2a_4$ corresponds to 5, 7, 15, and 24 h immersion times of Au-1,6HDT-SAM modified electrodes in a 0.50 mg/mL $AuNR_1$ aqueous solution (2.33 aspect ratio rods) at 35 °C. Similarly, $n = 2b_1$, $2b_2$, and $2b_3$ corresponds to 5, 15, and 24 h immersion time of Au-1,6HDT-SAM modified electrodes in a 0.50 mg/mL $AuNR_2$ aqueous solution (3.16 aspect ratio rods) at 35 °C. Obviously, the adsorption time of (self-assembly time) is equal to the immersion time of the Au-1,6HDT-SAM modified electrodes in AuNR solutions.

The SWVs and the CVs measured at the pure electrode $n = 0$, modified Au-1,6HDT-SAM electrode ($n = 1$), Au-1,6HDT-AuNR1 ($n = 2a_{1–4}$), and modified Au-1,6HDT-$AuNR_2$ electrodes ($n = 2b_{1–3}$) in an aqueous solution having 0.1 M $NaClO_4$ as the supporting electrolyte and 0.0005 M $[Fe(CN)6]^{3-/4-}$ as the redox probe. The 1,6-hexanedithiol has an insulating effect when self-assembled on gold electrodes [43–45]. This is confirmed by the vanishing of the Faradaic current at the modified Au-1,6HDT-SAM electrode ($n = 1$) as compared to the pure gold (Fig. 5, $n = 0$), proving a dense packing of the 1,6HDT molecules on the gold electrode surface. In other words, the 1,6HDT-SAM is blocking the electronic communication blocked between $[Fe(CN)_6]^{3-/4-}$ in solution and the underlying gold electrode surface. The author has proven the diffusion of the supporting electrolyte (0.1 M $NaClO_4$) through the 1,6HDT monolayer was highly hindered, as via cyclic voltammetry analysis.

During the electrochemical analysis the $NaClO_4$ revealed no evident effect on the bilayers' structure. The successive self-assembly of AuNRs onto modified Au-1,6HDT-SAM electrodes is switched to an efficient path for electron transfer from the $[Fe(CN)6]^{3-/4-}$ redox probe in solution toward the underlying gold electrode surface. High peak currents and decreased peak separation were measured using both Au-1, 6HDT-AuNRs modified electrodes through CVs. Depending on the immersion time of Au-1, modified 6HDT-SAM electrodes in an aqueous solution of AuNRs, the peak currents in the CVs analyzed at Au-1, modified 6HDTAuNRs electrodes enhanced with the immersion time but started to reduce after 24 h. The largest improvement of the electrical current in the cyclic voltammograms was measured after 7 h of chemisorption of $AuNR_1$ ($n = 2a_2$) or 15 h of chemisorption of $AuNR_2$ ($n = 2b_2$, Fig. 6a) onto Au-1,6 HDT-SAM electrodes. This indicates the optimum time of AuNRs self-assembly onto Au-1, modified 6HDT-SAM electrodes in order to attain a highest enhancement of the electrochemistry of $[Fe(CN)_6]^{3-/4-}$ probes at the modified electrodes [45].

C.C. Lin [46] reported enhanced CV using 1-D AuNRs. The ordered gold nanorod arrays show anodic peak currents (i_{pc}) of −6.5 mA, whereas i_{pc} of the disordered gold nanorods is −5.2 mA and that of the macroscopic flat electrodes is −3 mA. Gold-coated flat working electrode surface is available only by linear diffusion and ions on the flat working electrode surface may be basically trapped only on the surface area of active electrochemical reactions. The 1-D nanostructure of ordered nanorods open up the possibility of creating radial diffusion, and also that the radius of curvature of the individual nanorods results to more active diffusion for ions binding in equilibrium with the nanorods. Additionally, the surface area of arrayed AuNRs is much higher than those of flat working electrode. The disordered AuNRs showed an enhanced cyclic voltammetric response than that of macroscopic flat electrodes, only less important than that of ordered 1-D AuNRs. Less exposure surface area and more inter- contacts between nanorods than those of 1-D ordered gold nanorods may be the reason for the less significance.

Gold nanorod-based non-enzymatic electrochemical sensor for small molecules

Hydrogen peroxide

Munshi et al. [47] prepared magnetite (Fe_3O_4) coated AuNRs of two aspect ratios as active glassy carbon electrode modifiers for the fabrication of H_2O_2 electrochemical sensor. The AuNR-Fe_3O_4 nanohybrids of a smaller aspect ratio (1.6) outperform the longer AuNRs (aspect ratio 7.5) in the electrochemical detection of H_2O_2, as measured using CV and amperometry techniques. Both short and long AuNR-Fe_3O_4 hybrid materials on modified electrode showed higher electrochemical responses for the reduction of 2 mM H_2O_2 in phosphate buffer (pH 7.4) compared to Fe_3O_4 nanoparticles alone. A current response of approximately +60 to −110 μA for the short AuNR-Fe_3O_4 hybrid material was found to be around 5 times greater than that of the long AuNR-Fe_3O_4 hybrid material (+10 to −20 μA). With increasing concentration of H_2O_2, both the reduction and oxidation currents rise gradually for both materials between +0.6 and −0.6 V applied potentials. The current responses of both shorter and longer AuNR-Fe_3O_4 on GC electrodes increased steadily due to the electrocatalytic activity associated with H_2O_2 reduction. The overall current response showed a good linear correlation in the concentration range from 0.5 μM to 7.45 mM with correlation coefficients of 0.995 and 0.979

for short and long AuNR-Fe_3O_4 modified GC electrodes, respectively. The sensitivity of short and long AuNR-Fe_3O_4 nanohybrid was calculated to be 120 nA.mM^{-1} and 18 nA.mM^{-1}, respectively. Unfortunately, this is not the correct unit for electrochemical sensitivity and this makes data not comparable to other data. The limit of detection (LOD) of short and long AuNR-Fe_3O_4 modified GC electrodes were observed to be 3.2 μM and 13 μM (S/*N* = 3), respectively. There are two important properties associated with the changes in aspect ratio of the AuNR-Fe_3O_4 hybrid systems which could govern the overall sensing response, total surface area and uniform coating of the Fe_3O_4 nanoparticles. The short AuNR-Fe_3O_4 had a total surface area (~12,000 nm^2) of approximately 3 times larger than the long AuNR-Fe_3O_4 (~4000 nm^2), thereby contributing to its higher response. During reproducibility studies, the response currents of 1 mM H_2O_2 for five replicate amperometric measurements in phosphate buffer for the same short AuNR-Fe_3O_4 modified GC electrodes yielded the retention of 94% of the initial values. The nanohybrid showed the current response with high retention of 93% of the initial values after one month confirming the high stability of short AuNR-Fe_3O_4 modified GC electrode. Authors tested the selectivity with possible interfering species such as glucose, ethanol and citric acid, which are often present with H_2O_2 in typical samples. The steady-state current was measured upon successive addition of 0.25 mM H_2O_2 and 0.5 mM of one interfering species at a time into phosphate buffer and the results portrayed negligible to no interference by glucose, ethanol and citric acid. However, significant interference was observed in the presence of ascorbic acid.

S. Jayabal et al. [48] reported a synthetic method for the preparation of bimetal core/shell Au/Ag NR embedded in amine functionalized silicate sol–gel matrix (Au_{core}/Ag_{shell}–TPDT NRs) in aqueous medium for the electrochemical detection of H_2O_2The AuNRs showed an average length of 40 nm and a breadth of 11 nm with an aspect ratio of ~3.6. The TEM images of the Au_{57}/Ag_{43}–TPDT NRs showed an average length of 48 nm and a breadth of 18 nm with an aspect ratio of ~2.7 and a uniform coating of Ag shell on the AuNRs (Fig. 2a). The Au_{core}/Ag_{shell}–TPDT NRs modified electrode showed enhanced electrocatalytic activity towards H_2O_2 over other electrodes due to the synergistic effect measured between Au, Ag and silicate sol-gel (Fig. 2b). The amperometric determination of H_2O_2 at the Au_{57}/Ag_{43}–TPDT NRs modified GC electrode was performed at an applied potential of −0.7 V with a successive addition of 100 nM H_2O_2 in 0.1 M phosphate buffer (pH 7.2) (Fig. 2c). A linear relation was measured in the H_2O_2 concentration range of 100 nM to 1.2 μM with a correlation coefficient of 0.99 (*n* = 10) for the regression eq. I (nA) = 0.13 + 1.13 C (nM). The LOD and limit of quantification (LOQ) for H_2O_2 were estimated to be 40 and 120 nM, respectively. The modified electrode showed only a ~ 10% decrease in the catalytic current after one week which indicated good stability of the Au_{57}/Ag_{43}–TPDT NRs modified GC electrode in H_2O_2 detection.

Feng et al. [49] fabricated highly-dispersed Pt nanodots on AuNRs (HD- PtNDs@AuNRs) (Fig. 3a, b) with mimetic peroxidase activity as an active electrode modifier for the fabrication of H_2O_2 electrochemical sensor. The HD-PtNDs@AuNRs was synthesized by a seed-mediated growth approach. The HD-PtNDs@AuNR modified electrode displayed a high catalytic activity to H_2O_2 at −0.10 V (versus SCE), a rapid response within 5 s, a wide linear range of 2.0–3800.0 μM, a detection limit of 1.2 μM (S/*N* = 3), and a high sensitivity of 181 μA.mM^{-1}.cm^{-2} (Fig. 3c). These results suggested a promising potential of fabricating H_2O_2 electrochemical sensor using HD-PtNDs@AuNRs. The sensor was applied to the determination of H_2O_2 in the local lake water and the recoveries in the range of 91.7%–104.9% were determined. These results indicated the practical applicability and reliability of HD-PtNDs@AuNR/GCE in determining H_2O_2. Pang et al. reported [50] a novel non-enzymatic H_2O_2 sensor using graphene and AuNRs (GR − AuNRs) composite modified GC electrode. TEM analysis showed that the prepared AuNRs are quite uniform in shape and size with the average length and diameter about 39 and 13 nm. The composite modified electrode exhibited good performance in the electrocatalytic reduction of H_2O_2 and the sensor electrode showed a good linear dependence on H_2O_2 concentration in the range of 30 μM to 5 mM with a sensitivity of 389.2 μA.mM^{-1}.cm^{-2}. The LOD was estimated to be 10 μM.

Wang et al. [51] fabricated a novel hemoglobin (Hb) electrode modified with AuNRs and graphene oxide sheets (GOs) coated by polydopamine (Pdop) (GOs@Pdop) (Fig. 4a) and used for highly selective and sensitive determination of H_2O_2. The electrochemical characteristics of the sensor were studied using CV and chronoamperometry (Fig. 4b, c). The system was optimized to realize a reliable determination of H_2O_2 at −0.2 V with a detection limit of 2.0×10^{-6} M (S/*N* = 3). The apparent Michaelis-Menten constants ($K^{app}{}_M$) were calculated to be 0.13 mM for 0.70 mM for H_2O_2. It was found that the interferents Na^+, Cl^-, K^+, NO_3^-, CO_3^{2-}, SO_4^{2-}, Mg^{2+} and Ca^{2+} did not significantly disturb the H_2O_2 determination. The repeatability measurement for detecting 0.7 mM H_2O_2 using the same electrode showed a relative standard deviation (RSD) of 7.49% for H_2O_2. The stability of the sensor was also investigated and the peak current intensity only decreased 11.4% for H_2O_2 after 22 days. These results indicated that the modified electrode exhibited a high selectivity, good stability and good repeatability. Yang et al.

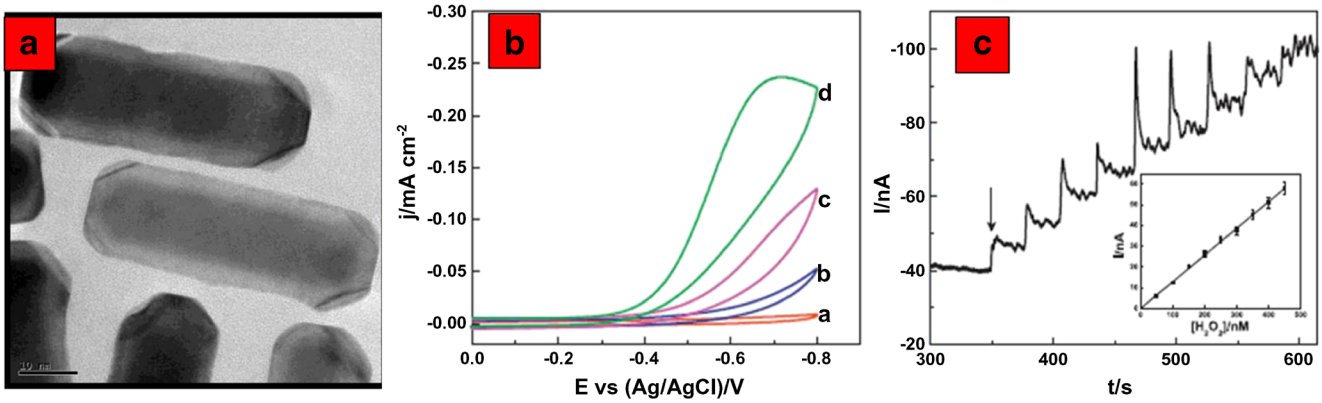

Fig. 2 **a** TEM image of Au_{57}/Ag_{43}-TPDT NRs; Fig. 2 (**b**) Cyclic voltammograms recorded for 1 mM of H_2O_2 at bare GC (**a**), GC/Au–TPDT NRs (**b**), GC/$Au_{75}Ag_{25}$-TPDT NRs (**c**) and GC/$Au_{57}Ag_{43}$-TPDT NRs (**d**) electrodes in 0.1 M PBS (pH 7.2) at a scan rate of 50 mV s^{-1}. Fig. 2 (**c**) Amperometric i-t curve obtained for H_2O_2 at GC/$Au_{57}Ag_{43}$-TPDT NRs modified electrode during the successive addition of 50 nM H_2O_2 to a stirred solution of 0.1 M PBS (pH 7.2) at an applied potential of −0.7 V. Fig. 2 (**c**) Inset: corresponding calibration plot [48]

[52] prepared Au_{core}/Ag_{shell} NR (Au@Ag NR) through the seed-mediated growth procedure using AuNRs as templates. The prepared Au@Ag NRs were used as a new electrode material for the construction of sensor by surface casting of Au@Ag NRs aqueous solution on a GC electrode. The fabricated sensor exhibited excellent catalytic performance for H_2O_2 reduction with a fast amperometric response time of less than 2 s, a wide linear response

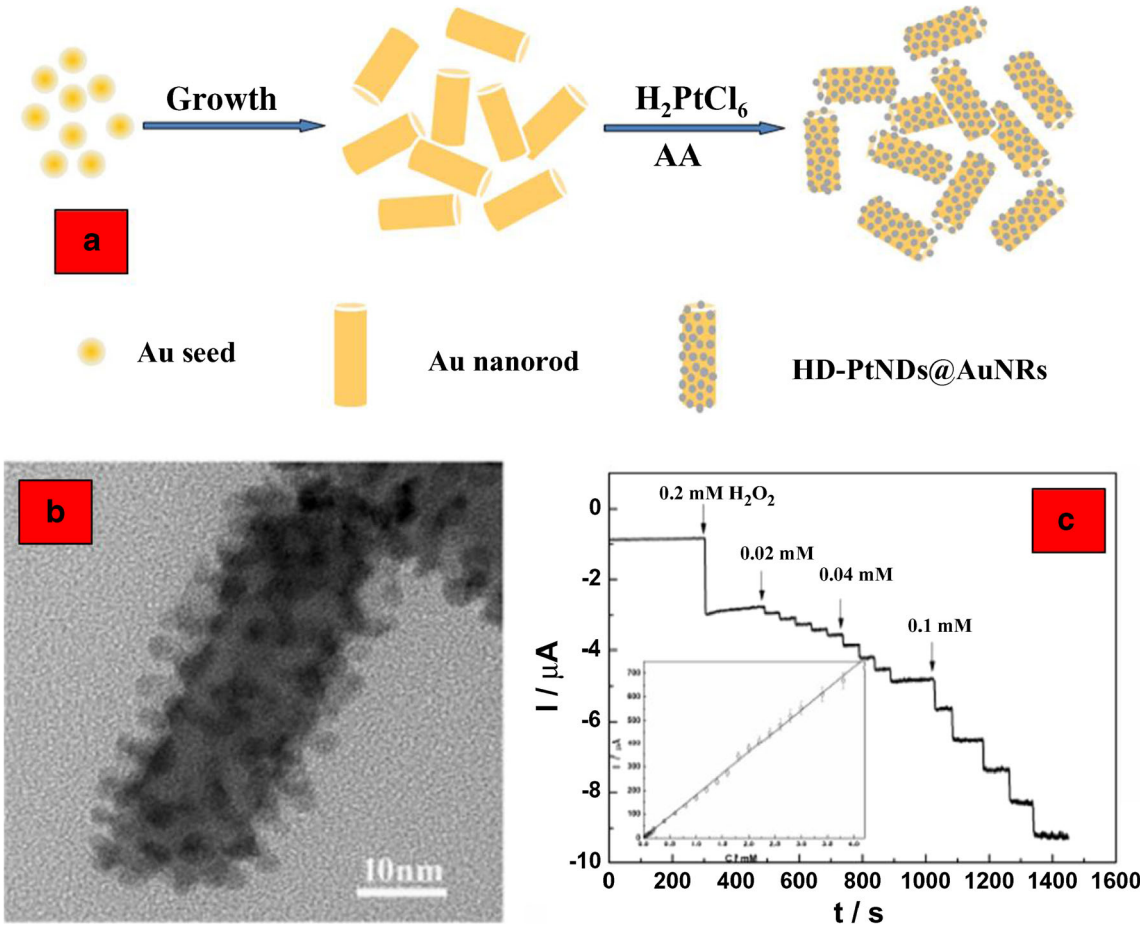

Fig. 3 **a** Illustration of preparation processes of HD-PtNDs@AuNRs; Fig. 3 (**b**) TEM image of HD-PtNDs@AuNRs; Fig. 3 (**c**) Amperometric response of HD-PtNDs@AuNRs/GCE on successive injection of H_2O_2 into the stirring N_2-saturated PB solution (0.01 M, pH 7.4). Applied potential: - 0.1 V. Fig. 3 (**c**) Inset: plot of H_2O_2 current versus its concentration [49]

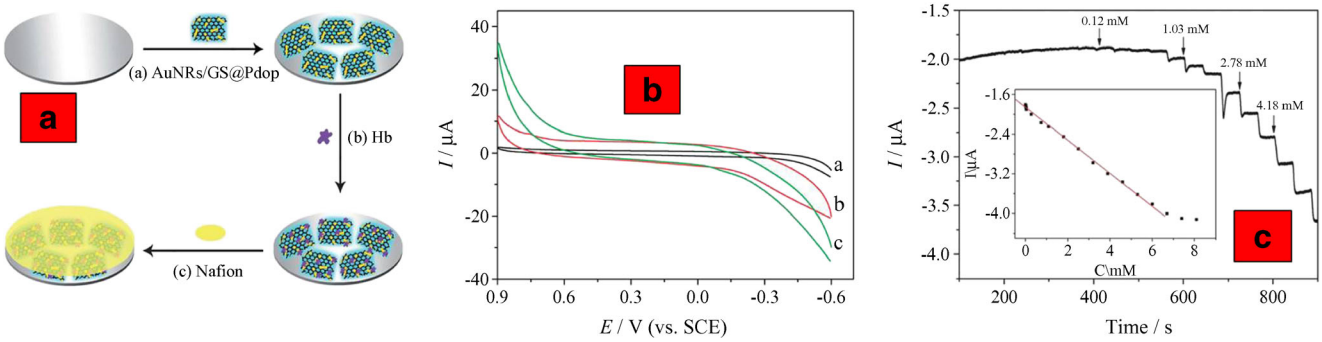

Fig. 4 **a** Illustration of the preparation process of the modified electrode; Fig. 4 (**b**) CVs of the Nafion/Hb/AuNR-GO@Pdop/GCE at a scan rate of 0.05 V s1 in buffer (pH 7.0) without H_2O_2 (a), with 77 mM H_2O_2 (**b**), and 87 mM H_2O_2 (**c**); Fig. 4 (**c**) Current-time response of the Nafion/Hb/AuNR–GO@Pdop/GCE with successive additions of H_2O_2 at pH 7.0 at an applied potential of 0.2 V. Fig. 4 (**c**) inset shows the linear calibration curve of H_2O_2 [51]

ranging from 0.02 to 7.02 mM (R = 0.99), and a LOD of 0.67 μM estimated on a signal-to-noise ratio of 3.

Nitric oxide

Nitric oxide (NO) is a diatomic molecule and free radical, which is endogenously prepared by a family of enzymes called nitric oxide synthases (NOSs) with L-arginine and O_2 as substrate [53, 54]. Nitric oxide (NO) acts a significant role in our daily life and has been extensively employed as an additive and a corrosion inhibitor in foods and beverages and physiological systems. The excess or deficiency of NO causing different pathological conditions including atherosclerosis, tumor angiogenesis, diabetes and Parkinson's disease [55]. Hence, the precise determination of NO is of great importance. S. Jayabal et al. [55] synthesized a graphene oxide–AuNRs embedded in functionalized silicate sol–gel matrix (RGO–Au–TPDT NRs) for the electrochemical sensing of nitric oxide (Fig. 5a). The TEM images of RGO–Au–TPDT NRs showed an average length of 49 nm and a breadth of 15 nm with an aspect ratio of ~3.3. The electrocatalysis and amperometric detection of NO were performed at physiological pH using the RGO–Au–TPDT NRs modified electrode. The modified electrode showed synergistic electrocatalytic effect of the RGO–Au–TPDT NRs composite for the oxidation of NO (Fig. 5b). The amperometric current response increased linearly with increasing the NO concentration in the range of 10–140 nM and the LOD was estimated to be 6.5 nM for NO detection (Fig. 5c). In another report, Marlinda et al. [56] fabricated a myoglobin (Mb)-modified AuNRs incorporating reduced graphene oxide (rGO) and deposited on a GC electrode to obtain a sensor for NO (Fig. 6). The nanohybrid modified GC electrode showed a distinct current enhancement in LSV for the determination of NO. The sensor, best operated at a working voltage of 0.85 V (vs. SCE), showed two linear response ranges from 10 to100 μM, and from 100 to 1000 μM in LSV, with a detection limit of 5.5 μM. It exhibited selectivity for NO over common interferents such as $NaNO_3$, and also over electroactive species such as ascorbate, dopamine, glucose, and uric acid.

Glucose

Glucose biosensor acts as an important role in the area of biological detection, clinical diagnosis and food production [57, 58]. U. Tamer et al. [59] fabricated polyaniline (PANI) film doped with colloidal gold nanorod particles electrode to immobilize glucose oxidase by glutaraldehyde. SEM images showed that the AuNRs have uniform morphology with average diameter and length of 15 nm and 45 nm, respectively. The amperometric response was measured as a function of concentration of glucose at a potential of 0.6 V versus Ag/AgCl in 0.1 M phosphate buffer at pH 6.4. Linear range of the calibration curve was from 17.6 μM to 1 mM with a sensitivity of 13.8 $\mu A.mM^{-1}.cm^{-2}$ and a LOD of 5.8 μM. The apparent Michaelis-Menten constant, K_M was calculated as 1.0 mM and the response time was less than 3 s.

L. Yingying et al. [60] prepared AuNRs by a seeding growth approach and used in fabricating the nanorod enhancing glucose biosensor. The high affinity of chitosan for AuNRs associated with its amino groups resulted in the formation of a layer of AuNRs on the surface of gold electrode. The performance of biosensors was investigated by CV, in the presence of artificial redox mediator, ferrocenecarboxaldehyde. The biosensor had a fast response to glucose, and the response time was less than 10 s. The results indicated that the AuNRs enhance the current response to glucose. The detection limits of glucose reached 10 mM, and the Michaelis-Menten constant app K_m^{app} is 13.62 mM. The linear response range of the sensor to the concentration of glucose can extend to at least to 10 mM (correction coefficient R = 0.971, n = 9) and the sensor had a high sensitivity of 1.517×10^{-5} $A.mM^{-1}.cm^{-2}$.

H. Ciftci et al. [61] achieved the immobilization of surface-functionalized self-assembled monolayer (SAM) gold

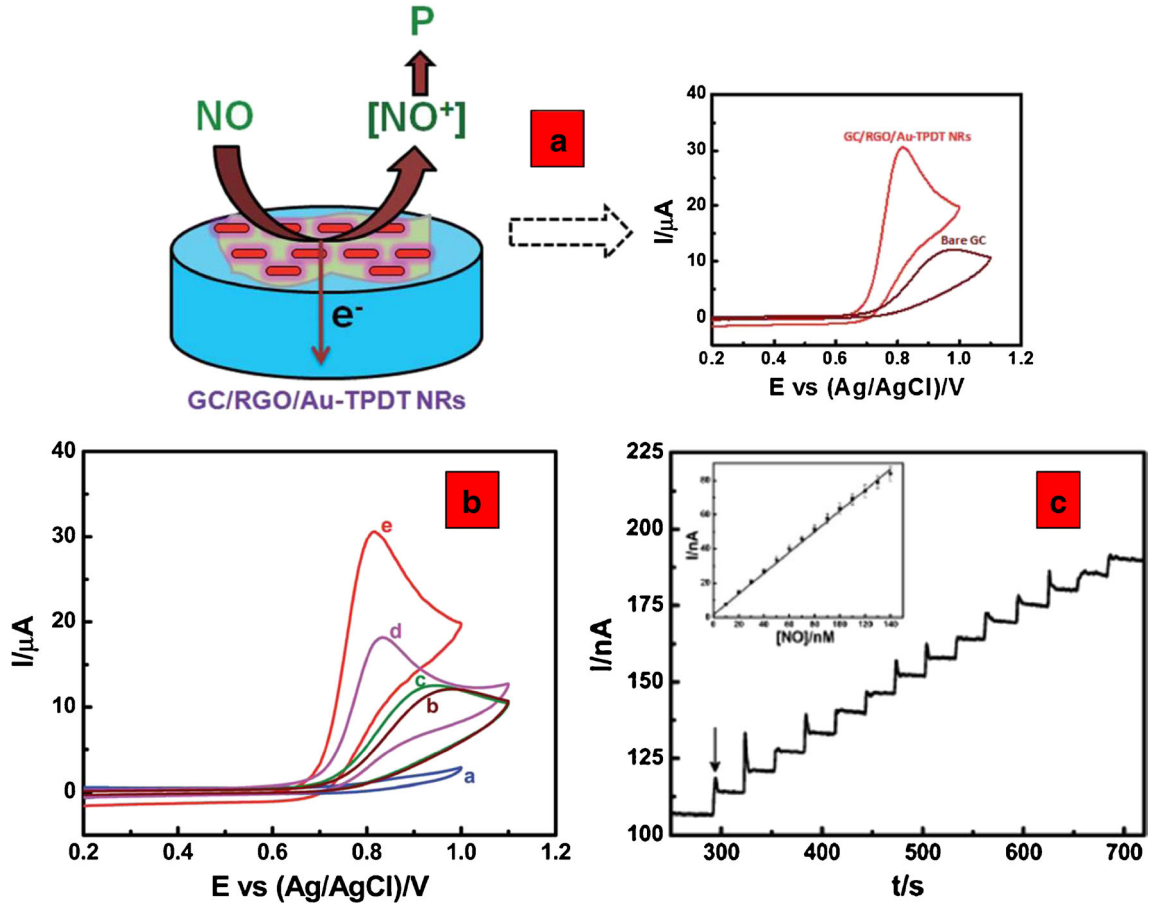

Fig. 5 **a** Schematic illustration of electrocatalytic oxidation of NO at the GC-RGO-Au-TPDT NRs modified electrode. (P-Products); Fig. 5 (**b**) Cyclic voltammograms recorded at GC-RGO-Au-TPDT NRs in the absence of NO (**a**) and in the presence of 10 mM NO at bare GC (**b**), GC–RGO–TPDT (**c**), GC-Au-TPDT NRs (**d**) and GC-RGO-Au-TPDT NRs (**e**) electrodes in buffer of pH 7 at a scan rate of 50 mV s1; Fig. 5 (**c**) Amperometric i-t curve obtained for NO at GC-RGO-Au-TPDT NRs modified electrode during the successive addition of 10 nM NO to a stirred solution of pH 7.2 at an applied potential of 0.8 V. Fig. 5 (C) Inset: corresponding calibration plot [55]

nanoparticles onto poly(3-octylthiophene) (POT) by the cooperation of hydrophobic forces. SAMs were prepared by 11-mercaptoundecanoicacid (MUA), 4-mercaptophenyl boronic acid (MPB), and 1-decanethiol (DT) hydrophobic substrates. POT-Au-SAM (MPB) electrode was used for glucose determination as potentiometric non-enzymatic glucose sensor. The analytical performance was evaluated and linear calibration graphs were measured in the concentration range of 5–30 mM glucose including the level of human blood glucose. The detection limit was calculated on the basis of signal-to-noise ratio of 3 was 0.2 mM. Ren et al. [62] fabricated amperometric glucose biosensor based on immobilization of glucose oxidase (GOx). The current response of modified electrode was 10 times higher than without AuNRs. Under optimal conditions, the biosensor showed high sensitivity of 8.4 $\mu A.cm^{-2}.mM^{-1}$, low detection limit of 2×10^{-5} M, good

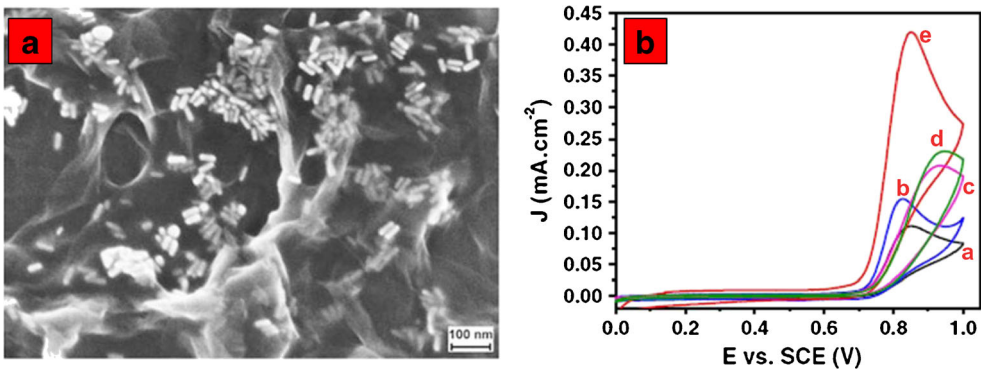

Fig. 6 **a** FESEM image of Mb-AuNR/rGO sample; Fig. 6 (**b**) Cyclic voltammograms obtained for bare GCE (**a**), AuNRs/GCE (**b**), rGO/GCE (**c**), Mb/GC (**d**), and Mb-AuNR/rGO/GCE in buffer of pH 2.5 with 1 mM NO at the scan rate of 50 $mV.s^{-1}$ [56]

storage stability and high affinity to glucose (K_m^{app} = 3.84 mM). A linear calibration plot was measured in the wide concentration range from 3×10^{-5} to 2.2×10^{-3} M. The reproducibility of response current of the GOx enzyme electrode was investigated at a glucose concentration of 2.2 mM. The relative standard deviation (RSD) of the biosensor was 2.3% for 10 successive measurements. The RSD for five biosensors were prepared at same conditions was 7.2%. The stability of the enzyme electrode was also investigated by amperometric measurements in the presence of glucose with 2.2 mM over a month period. The current response of biosensor retained about 80% of its original response after storing.

Hsu et al. fabricated [63] a highly sensitive Au-Ni coaxial nanorod array electrode through the integration of nano electroforming and immersion gold (IG) method for glucose detection. The average diameter of the synthesized Ni nanorods and that of the Au-Ni nanorods were estimated to be 150 and 250 nm, respectively; both had a height of 30 μm. The aspect ratio was 120. Compared to that of a flat gold electrode, the effective sensing area was enhanced by 79.8 fold. Fig. 7a and b depicts cyclic voltammograms and amperometric curves for various glucose concentrations. Actual glucose detections demonstrated that the prepared Au-Ni coaxial nanorod array electrode works in a linear range from 27.5 μM-27.5 mM with a detection limit of 5.5 μM and a very high sensitivity of 769.6 $\mu A.mM^{-1}.cm^{-2}$. Good selectivity of the fabricated sensing device was verified by sequential injections of uric acid (UA) and ascorbic acid (AA). Long-term stability was examined through successive detections over a period of 30 days. H. Liu et al. [64] prepared a new glucose biosensor based on the electron transfer and photothermal effect of AuNRs. The biosensor was prepared by immobilizing glucose oxidase (GO*x*) on a Pt electrode by a composite film consisting of gold nanorods (AuNRs), poly(vinyl butyral) (PVB) and glutaraldehyde. AuNRs were synthesized by gold seed-mediated cetyltrimethylammonium bromide (CTAB) surfactant-assisted approach. With increasing glucose concentration, the amperometric response increased. When the GO*x* concentration is 22 mM, the current response of the Pt/GO*x*/PVB electrode is 3.6 $\mu A.cm^{-2}$. In contrast, that of an electrode with AuNRs is 15.5 $\mu A.cm^{-2}$. The average current response of a AuNR-modified enzyme electrode without NIR irradiation is 10.5 $\mu A.cm^{-2}$. With the increase in laser power density, the current response of the AuNR-modified enzyme electrode is enhanced. When the laser power density reaches 25.5 $mW.cm^{-2}$, the current response of the AuNR-modified enzyme electrode is 23.2 $\mu A.cm^{-2}$, which is more than twice the initial current response of a AuNR-modified enzyme electrode without NIR irradiation.

Dopamine

Dopamine (DA) is one of the most considerable catecholamines and acts a main role in neurotransmission. The fast and precise determination of DA is of great importance in the diagnosis of neurological disorders including Huntington's disease, Parkinson's disease, autism, schizophreni [65, 66]. M. Ahn et al. [65] studied the electrochemical behavior of dopamine (DA) at dendritic gold rod (DAR) surfaces prepared through electrodeposition from sulfite-based Au(I) electrolytes. SEM images showed that the DAR structures were homogeneously formed on a large-scale throughout the entire electrodeposited area (>6.6 mm^2), and the color of the DAR surface was dark brown, indicative of formation of nanoscale gold structures. The height of the DAR structures spanned from 150 to 250 nm, and the individual DARs retained highly faceted star-shaped protrusions on the sub-100 nm scale. The unique electrochemical behavior of DA at DAR surfaces enabled the DPV determination of DA in the ranges between 1 and 12 μM in the presence of 0.1 mM of AA. The peak currents

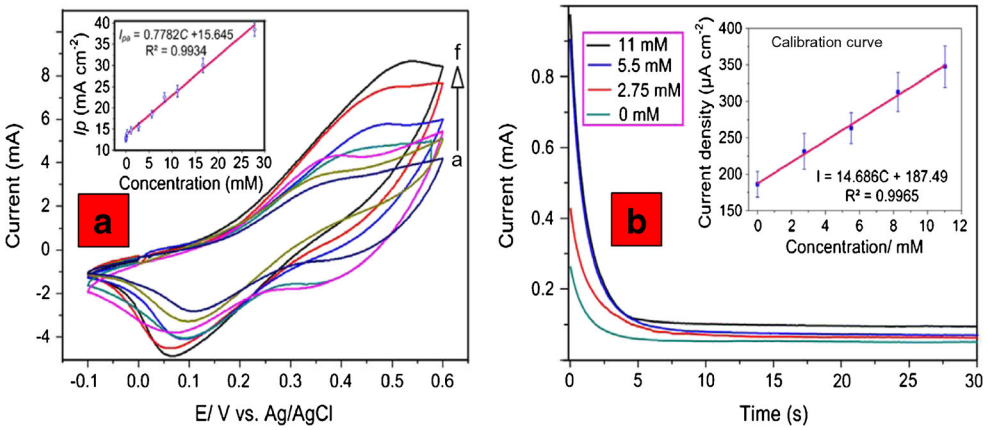

Fig. 7 **a** Cyclic voltammogram for various glucose concentrations with curves a to f representing the concentrations of 0, 0.0275, 5.5, 11, 16.65, and 27.5 mM, respectively. (Fig. 7 (**a**) inset) Linear calibration curve representing the peak current and concentration relationship; Fig. 7 (**b**) amperometrics for different glucose concentrations with 0, 2.75, 5.5, and 11 mM. Fig. 7 (**b**) (inset) linear calibration curve represents the relationship between the steady-state current and glucose concentration [63]

for DA oxidation in the DPV were not affected by the presence of AA in concentration ranges up to 0.2 mM. In the presence of 0.1 mM AA, the peak currents of DA oxidation linearly increased with the concentration of DA up to 12 μM (Fig. 6b). The sensitivity of the calibration plot measured 7.4 L $\mu A.\mu M^{-1}.cm^{-2}$, and the detection limit was estimated to be ~1 μM. The existence of the highly-faceted edge sites on the DAR surfaces played an important role for the electrochemical detection of DA at gold -based electrode surfaces.

C. Deng et al. [66] prepared AuNRs/multiwalled carbon nanotubes (CNT) composite film-modified glassy carbon (GC) electrode by the electrostatic interaction between the positively charged AuNRs and the negatively charged CNT. The AuNRs/CNT/GC electrode was used for the selective and sensitive determination of dopamine (DA) in the presence of ascorbic acid (AA). In CV, one broad voltammetric signal was observed for both 1 mM AA and 0.1 mM DA analytes, and the mixed voltammetric signals were resolved into two voltammetric peaks, and it might be feasible to carry out the electrochemical detection of DA in the presence of AA. Two well-defined and shape DPV peaks with respect to AA and DA oxidation appeared at −0.08 V and 0.155 V with a potential separation of 235 mV, which was sufficient enough for the determination of DA in the presence of AA and well avoids the co-oxidation of AA and DA at the same potential window. The oxidation potentials of DA and AA based on the gold nanoparticles modified gold electrode were 0.015 and 0.185 V, and the peak separation between the voltammetric peaks of AA and DA was 165 mV. The oxidation of AA and DA at a wide potential separation in the AuNRs/CNT/GC electrodes may be due to the synergic effect of AuNRs and CNT. In order to investigate the stability of the electrode, the amperometric response of 0.3 μM DA was recorded once in every hour. The current responses for six injections remained almost constant and the relative standard deviation of 5.6%. Also, there were no obvious changes in the response of the AuNRs/CNT/GC electrode after its storage in phosphate buffer solution for a week. In order to verify the reliability of the method for practical analysis of DA, the AuNRs/CNT/GC electrode has been used to determine DA in healthy human blood serum. The recovery was found ranged from 97.5 to 101.5. From the experimental results, it was noted that the presence of AA, UA and some other interference, such as albumin and glucose did not interfere with the determination of DA during real sample analysis. Z. Jia et al. [67] synthesized AuNRs using a template technique and then dispersed in a saturated sodium citrate solution by ultrasonication to form AuNRs suspension. The TEM image showed that the individual AuNRs can be basically dispersed although some certain linkage of several AuNRs still exists. The surface of AuNRs was rather smooth and the diameters were quite uniform, which were about 10 nm. The average length is about 100 nm, and the aspect ratio (the ratio of the length to the diameter) is about 10:1. The SWVs and calibration curve for dopamine at the AuNR/GC electrode are displayed in Fig. 4. The linear concentration range of dopamine was 1×10^{-8} M to 1×10^{-7} M. The current sensitivity was 3.280 $\mu A.\mu M^{-1}$. The detection limit (s/n = 3) was as low as 5.5×10^{-9} M.

NAD^+ and NADH

Reduced β-nicotinamide adenine dinucleotide (NADH) and its oxidized form NAD^+ are most important coenzymes in the energy production of living cells. The NADH/NAD^+ redox system plays a crucial role in the electron transfer process and charge carrier with in the biological system. The electrochemical detection of NADH by direct oxidation with conventional electrodes requires a high over potential. Li et al. [68] reported a strategy for the preparation of AuNRs incorporated graphene nanosheets (GN- AuNRs) through electrostatic interaction for the amperometric detection of NADH. The GN- AuNRs modified electrode showed well catalytic oxidation current of NADH which is a slight negative shift of the onset potential for the NADH oxidation on the bare GC. The origin of synergism is due to the combination of GN and AuNRs. The distribution of AuNRs makes close contact with graphene sheets hence the electron transfer was influenced thus enhance NADH oxidation. The GN-Au NR electrode showed an amperometric response to the successive addition of NADH within 10 s in the linear ranges 20–480 μM with the LoD of 6 μM (S/N = 3). Moreover the GN-AuNRs electrode showed good repeatability and stability owing to the capability to minimize the surface fouling of electrode after NADH oxidation. S. Jayabal et al. [69] prepared AuNRs stabilized in amino-functionalized silicate sol–gel matrix (Au–TPDT NR) in aqueous medium and applied it for the electrochemical sensing of reduced β-nicotinamide adenine dinucleotide (NADH) (Fig. 8a-c). The amperometric sensing of NADH showed enhanced electrocatalytic activity for the Au-TPDT NRs modified electrode without incorporating any mediator. The amperometric current increased linearly with increasing the NADH concentration in the range from 1 to 13 μM and the lowest detection limit was estimated as 0.38 μM. A linear relationship with a correlation coefficient of 0.99 (n = 13) for the regression eq. I (nA) = 10.47 + 1.37 C (μM) was analyzed for NADH concentration in the range from 1 to 13 μM with a sensitivity of 10.47 $nA.\mu M^{-1}$. The response time was found to be 3 s and this indicated the presence of a fast electron transfer process at the modified electrode. The LOD and LOQ values were estimated as 0.38 and 1.15 μM, respectively, for the NADH at GC/Au–TPDT NRs modified electrode.

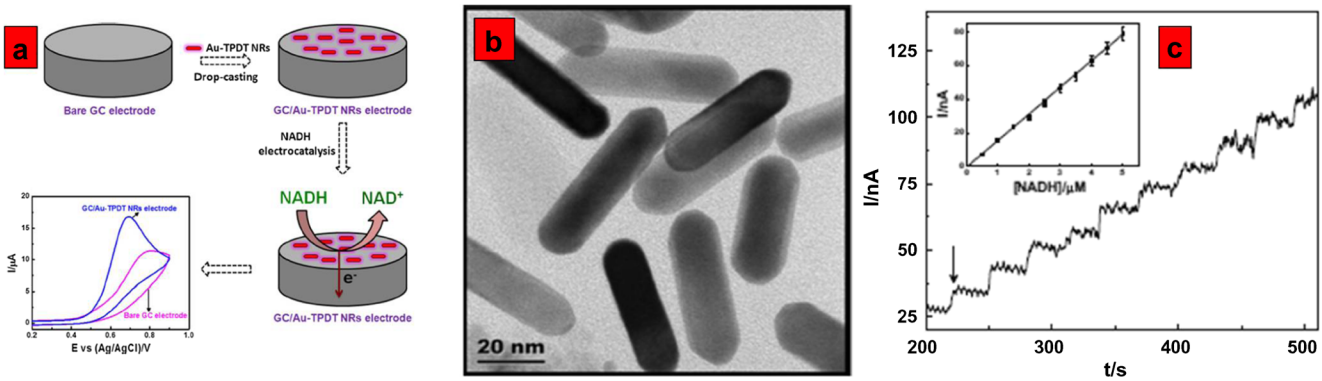

Fig. 8 **a** Schematic illustration of electrocatalytic oxidation of NADH at the GC/Au–TPDT NRs electrode; Fig. 8 (**b**) TEM image of Au-TPDT NRs; Fig. 8 (**c**) Amperometric i-t curve obtained for NADH at GC/Au-TPDT NRs modified electrode during the successive addition of 0.5 lM NADH to a stirred solution (pH 7.2) at an applied potential of 0.7 V. Fig. 8 (**c**) Inset corresponding calibration plot [69]

L-cysteine

Cysteine (Cys) is sulfur containing non-essential important aminoacid and present in natural proteins, which acts as important roles in biological systems. Cys plays as cancer indicator, antioxidant, radio protective agent, antitoxin and free radical scavenger. The deficiency of Cys results in various pathological conditions such as skin lesions, edema, slowed growth in children, hair depigmentation, liver damage, muscle and fat loss and weakness [70]. Hence, sensitive determination of Cys has become important for physiological and clinical diagnoses. F.A.S. Silva et al. [70] fabricated a nanohybrid consisting of multi-walled carbon nanotubes and AuNR modified GC substrate for the electrocatalytic oxidation of L-cysteine (Cys). Oxidation of Cys was measured through CV results by the modified electrode, which showed Cys at a very low anodic potential (0 V vs. Ag/AgCl). The low oxidation potential, better sensitivity, low detection limit (8.25 nmol.L^{-1}), higher k_{cat} and good sensitivity of 120 nA.L.μmol^{-1} can be attributed to the efficiency of the electron transfer between the nanohybrid modified surface and Cys. The determination of Cys in human serum was performed to examine the applicability of the present electrochemical sensor in biological samples. The recovery test was also studied by spiking the serum samples with 50 μmol.L^{-1} of Cys into 0.1 mol.L^{-1} pH 7.0 phosphate buffer solution. The recoveries were from 99.7% to 100.4%, indicating that the method was highly accurate, with relative standard deviation, from 2.3 to 4.2%, indicating an acceptable reproducibility. The detection limit of the sensor is in accordance with the concentration range of free Cys in human serum, which are in healthy people, from 7 to 59 μmol.L^{-1}.

Other analytes

Narang et al. [71] prepared AuNRs for the amplification of electrochemical sensing of anti-HIV replication drug i.e. deferiprone. AuNRs deposited on pencil graphite electrode (PGE) was utilized for covalent immobilization of horse radish peroxidase (HRP),via glutaraldehyde (Glu), for deferiprone detection using impedimetric technique. The resulting nano gold sensor exhibited a good response to deferiprone with a wide linear range (0.005–1000 mM) and a low detection limit 0.005 mM. The biosensor also showed a short response time (within 15 s). In addition, the biosensor exhibited high reproducibility, good storage stability and selectivity. The applicability of the nano gold sensor is to determine deferiprone level in spiked urine and serum samples.

W. Bai et al. [72] synthesized well-dispersed graphene/gold nanorod (G/AuNR) composites by directly reducing a mixture of graphene and gold growth solution with sodium borohydride. GC electrode was modified with G/AuNR composite for the detection of ractopamine based on the strong enhancement effect of G/AuNRs. The peak currents varied linearly with the concentration of ractopamine over the range of 1×10^{-9} to 2.7×10^{-6} mol.L^{-1}, and the detection limit was 5.1×10^{-10} mol.L^{-1} (S/*N* = 3). This method was applied to detect the content of ractopamine in swine urine samples, and the recovery was in the range of 99.2 to 107.3%. The RSD of each sample for three parallel detections was less than 5.1%, and the results measured by the G/AuNR/GCE device were acceptable.

Rahi et al. [73] designed a sensitive electrochemical sensor based on AuNRs synthesized by a sonoelectrodeposition method. Nitrofurazone was electroreduced on the nanorod surface at lower potentials with a higher rate, compared to a polycrystalline smooth gold surface, through an irreversible process. The results showed that the nanorods could be utilized to fabricate a nitrofurazone sensor. Amperometric and differential pulse voltammetric procedures were applied to the determination of nitrofurazone. Linear dynamic ranges of 50–610 and 3.0–500 μmol.L^{-1} with calibration sensitivities of 2.02 and 0.5 A.L.mol^{-1}.cm^{-2}, and detection limits of 6.51 and 0.18 μmol.L^{-1} were measured using amperometry and DPV, respectively. Dong et al. [74] fabricated, layer-by-layer self-assembly of positively charged cetyltrimethylammonium

bromide (CTAB) wrapped AuNRs and negatively charged superoxide dismutase (SOD) from their aqueous solutions on cysteine modified gold electrode (Cys/Au), a third generation electrochemical biosensor $(SOD/AuNR)_2$/Cys/Au) for superoxide anion ($O_2^{\cdot-}$). The two layers assembly of SOD/AuNR significantly enhanced the direct electron transfer between SOD and the electrode. The functional enzymatic activities of the SOD offer an electrochemical approach to the determination of $O_2^{\cdot-}$. In the reductive regions, the fabricated sensor exhibited excellent analytical performances, such as wide linear range (200 nM to 0.2 mM $O_2^{\cdot-}$), low detection limit (100 nM $O_2^{\cdot-}$), high sensitivity (22.11 $nA.cm^{-2}.\mu M^{-1}$), short response time (less than 5 s), good stability and reproducibility, while no obvious interferences are caused by commonly met interfering species including H_2O_2, UA and AA.

M. Arvand et al. [75] reported a novel, and selective electrochemical method for the determination of indomethacin in aqueous media (phosphate buffer, pH 8.0) on AuNR-GO nanocomposite incorporated carbon nanotube paste modified GC electrode (AuNRs–GO–CNTP/GCE) using SWV. The AuNR-GO-GO-CNTP/GCE displayed high effective surface area, more reactive sites and excellent electrochemical catalytic activity toward the oxidation of indomethacin. The detection limit of 1.7×10^{-2} μM and two linear calibration ranges of 0.2–0.9 and 2.5–91.5 μM were determined for indomethacin determination at AuNR-GO-CNTP/GCE. The fabricated modified electrode was successfully applied for the determination of indomethacin in human blood serum, urine and pharmaceutical samples. A typical SWV of the human blood sample at AuNR-GO–CNTP/GCE showed the well-defined oxidation peak of indomethacin at ca. 0.52 V. The blood sample of the patient was then spiked with known concentrations of indomethacin and the voltammograms clearly depicted that the peak currents increase significantly for the peak at ca. 0.52 V. The recovery was measured from 98.0% to 103.5%. The results showed that there is a satisfactory agreement between the declared analyte content and the determined value. Table 3 displays the summary of analytical performance of some Au nanorods and its composite modified electrode for the detection of hydrogen peroxide, nitric oxide, glucose, dopamine, NAD^+ and NADH, L-Cysteine and other analytes.

Gold nanorod based enzymatic electrochemical sensing of small molecules

S. Komathi et al. [76] reported a one-pot procedure for simultaneously immobilizing horseradish peroxidase (HRP) and poly(N-[3-(trimethoxysilyl)propyl]aniline (PTMSPA) on AuNRs (Fig. 9a). High resolution image of HRP/PTMSPA@AuNR attributes AuNRs are welded/connected to one another through the surface coated PTMSPA. CVs of H_2O_2 at HRP/PTMSPA@AuNR modified electrode exhibited a stable reduction peak at approximately −0.25 V. Amperometric response of HRP/PTMSPA@AuNR modified electrode showed quick response (<5 s) for the reduction of H_2O_2. HRP/PTMSPA@AuNR showed wide linear range from 1×10^{-5} to 1×10^{-3} M with detection limit (0.06 μM) ($S/N = 3$) (Fig. 9b). HRP/PTMSPA@AuNR modified electrode exhibited high selectivity with sensitivity 0.021 $\mu A.\mu M^{-1}$ toward H_2O_2. S. Zhang et al. [77] fabricated a novel electrochemical glucose sensor based on Au@Ag heterogeneous nanorods (Au@Ag heterogeneous NRs). The Au@Ag heterogeneous NRs exhibited favorable electrocatalytic ability to reduce H_2O_2 at negative potential of about −0.6 V (vs. SCE). Further, the glucose oxidase (GOx)/Au@Ag heterogeneous NRs modified electrode was constructed as a glucose sensor, which exhibited wide linear range of 0.02–10 mM glucose in O_2 saturated phosphate buffer at an applied potential of −0.4 V and and a low detection limit of 1.5 μM in a ratio of signal to noise of 3. In addition to good reproducibility and stability, the sensor exhibited good selectivity to common interferents such as AA, UA and DA, other saccharides, and 0.15 M chloride ions. The sensor was further used to detect glucose in human serum samples. The recoveries of three serum samples after addition of standard glucose were within 97.4–102.3%, indicating that the method was very accurate.

Li et al. [78] constructed a new glucose biosensor by immobilizing glucose oxidase (GOx) in the Chitosan (Chit)-MWCNTs/AuNR composite membrane. The Chit-MWCNTs/GOx /AuNR/gold electrode (GE) displayed a pair of well-defined and reversible redox peaks with the formal potentials (E_0) of -0.384 V in 0.1 $mol.L^{-1}$ pH 7.0 phosphate buffer solution. The surface concentration (Γ^*) of the electroactive GOx in the film was estimated to be $(7.03 \pm 0.02) \times 10^{-11}$ $mol.cm^{-2}$. The electrocatalytic oxidation to glucose of Chit-MWCNTs/GOx/AuNR/GE was also studied. Its apparent Michaelis-Menten constant for glucose was 1.34 $mmol \cdot L^{-1}$. The experiment results showed that the linear dependence of the electrocatalytic current of the biosensor was from 0.28 to 5.88 $mmol \cdot L^{-1}$, the detection limit of the sensor was 2.06×10^{-5} $mol.L^{-1}$ ($S/N = 3$), and the sensitivity was 38.2 $\mu A.mmol^{-1}.cm^{-2}$. Moreover, the biosensor showed rapid response to glucose, good stability and reproducibility. Nirala et al. [79] fabricated a potential bioelectrode material by immobilizing glucose oxidase on reduced graphene oxide–gold nanorods supported by chitosan (CH- prGO-AuNR) for enhanced glucose sensing. These CH–prGO–AuNR/ITO bioelectrodes demonstrated high sensitivity of 3.2 μA/(mg/dL)/cm^2 and linear range of 25–200 mg/dL with an ability to detect as low as 14.5 mg/dL. Further, these CH-prGO-AuNR/ITO based electrodes attest synergistically enhanced sensing properties. Additionally, very low K_m value [15.4 $mg.dL^{-1}$ (0.85 mM)] ensures better binding affinity of enzyme to substrate which is desirable for good biosensor stability and

Table 3 Summary of analytical performance of some Au nanorods and its composite modified electrode for the detection of different analytes

Analyte	Electrode material	Fabrication method	Detection method	Linear range	Limit of detection	Interference	Ref.
Hydrogen Peroxide	AuNRs-Fe_3O_4	electrostatic interaction mediated self-assembly process	CV, AMP	0.5 μM to 7.45 mM	3.2 μM and 13 μM	Glu, ethanol, AA, citric acid	[47]
	Au/Ag nanorods	seed-mediated growth method	CV, AMP	100 nM to 1.2 μM	3.3(SD/S)	Glu, urea, and oxalate	[48]
	HD- PtNDs@AuNR	seed-mediated growth	CV, CA	2.0–3800.0 μM	1.2 μM	AA, UA	[49]
	GR-AuNR	Seed-mediated growth method	CV, CA	30 μM to 5 mM	10 μM	phenolic acids, flavonoids	[50]
	AuNR-GOs@Pdop	In situ spontaneous oxidative polymerization method	CV, CA	3.6–6000.0 μmol L^{-1}	200.0 μmol L^{-1}	Na^+, Cl., K^+, NO_3^-, CO_3^{2-}, SO_4^{2-}, Mg^{2+} and Ca^{2+}	[51]
	Au@Ag NRs	seed-mediated growth procedure	CV	0.02 to 7.02 mM	0.67 μM	AA, UA, DA	[52]
Nitric oxide	RGO-Au-TPDT	seed mediated growth method	CV, CA	10–140 nM	6.5 nM	Glu, urea oxalate, NaCl	[55]
	Mb-AuNR/rGO/GCE	seed mediated-growth solution	CV, LSV	10 μM to 1 mM	5.5 μM	AA, UA, DA, Glu	[56]
Glucose	PANI-AuNR Electrode	seed-mediated growth technique	CV, AMP	17.6 μM to 1 mM	5.8 μM	AA, UA	[59]
	AuNRs	seeding growth approach	CV, AMP	10 mM	10 mM	----------	[60]
	Self-assembled monolayer of AuNR	seed-mediated growth technique	CV	5 mM and 30 mM	0.2 mM	----------	[61]
	AuNRs/cellulose acetate film	seed-mediated growth	CV, CA	3×10^{-5} to 2.2×10^{-3} M	2×10^{-5} M	----------	[62]
	Au-Ni coaxial nanorod	Integration of nano electroforming and immersion gold (IG) method	CV	27.5 μM-27.5 mM	5.5 μM	UA, AA	[63]
	gold nanorods	seed-mediated	CV, AMP	--------	--------	--------	[64]
Dopamine	Dendritic AuNRs	electrochemical deposition	CV, DPV	12 μM	~1 μM	AA	[65]
	AuNR/MWCNTs	electrostatic reaction	CV, DPV	0.5×10^{-6} to 1.8×10^{-5} M,	0.8 nM,	AA, UA, albumin, Glu	[66]
	Gold nanorods	Anodic aluminum oxide (AAO) template	CV, SWV	1×10^{-8} M to 1×10^{-7} M	5.5×10^{-9} M	AA	[67]
NAD^+ and NADH	graphene-Au NR hybrid nanosheets	electrostatic interaction	CV, CA	20 to 160 μM (NADH) 5 to 377 μM (NAD+)	6 μM (NADH)and 1.5 μM (NAD+)	AA, UA, Glu	[68]
	Gold nanorods	seed-mediated growth method	CV, AMP and DPV	1 to 13 μM (NADH)	0.38 μM	AA	[69]
L-Cysteine	MWCNT/AuNRs	cationic surfactant-containing seed--mediated	CV, Chronoamperograms	5.0 upto 200.0 μmol L^{-1}	8.25 nmol L^{-1}	AA, UA, NADH	[70]
Deferiprone	Gold nanorods	seed-mediated method	CV, SWV	0.005–1000 μM	0.005 μM	------	[71]
Ractopamine	graphene/gold nanorod	seed-mediated chemical synthesis,	DPV	1×10^{-9} to 2.7×10^{-6} mol L^{-1}	5.1×10^{-10} mol L^{-1}	H2O2, DA, AA, UA, Glu, glycine	[72]
Nitrofurazone	gold nanorods	Sonoelectro-deposition method	CA, DPV	50–610 and 3.0–500 μmol L^{-1}	6.51 and 0.18 μmol L^{-1}	---------	[73]
Superoxide anion	$SOD/AuNR)_2$/Cys/Au	layer-by-layer self-assembly	CV, CA	200 nM to 0.2 mM	100 nM	H_2O_2, UA, AA, 5-HIAA, HVA, DOPAC	[74]
Indomethacin	AuNR-GO–CNTP/GCE	Three-step seed-mediated method	LSV, CA	0.2–0.9 and 2.5–91.5 μM	1.7×10^{-2} μM	Na^+, K^+, Ca^{2+}, Mg^{2+}, Cu^{2+}, Zn^{2+}, Fe^{2+}, Cl^-Niacin, glycine, alanine, starch, gelatin and aspartic acid, Glu, cysteine, lactose, AA, UA Tyrosine and tryptophan, Piroxicam	[75]

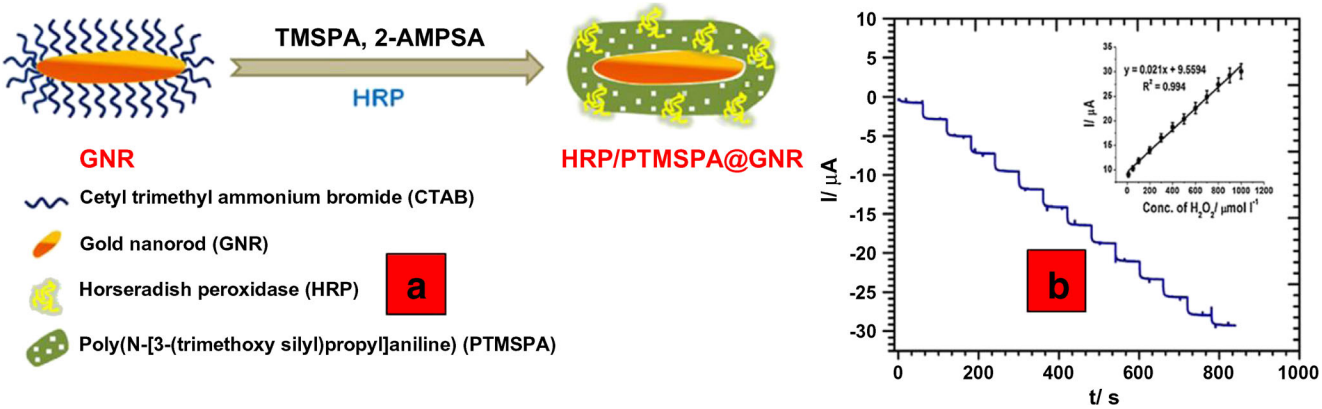

Fig. 9 **a** One pot synthesis of HRP/PTMSPA@AuNR; Fig. 9 (**b**) Amperometric response at HRP/PTMSPA@AuNR for successive addition of 20 L H_2O_2 in 0.1 M PBS (pH = 7.0) (applied E = −0.25 V); Fig. 9 (**b**) inset: Calibration curve [76]

resistance to environmental interferences. Table 4 shows the summary of analytical performance of some gold nanorod based enzymatic electrochemical sensor for the detection of small molecules.

Gold Nanorod based DNA biosensors

The development of a rapid, sensitive, cost-effective and sequence specific DNA detection method is highly desired for the early stage diagnosis of genetic diseases. DNA biosensors, also called as genosensors, are analytical devices produced from the integration of a sequence-specific probe and a transducer. Electrochemical DNA detection techniques present great improvement in DNA diagnostics as it offers accurate and inexpensive method in addition to the generation of direct electronic signal without requiring of expensive signal transduction equipments [80].

Han et al. [81] constructed an electrochemical sensor for sensitive and selective DNA detection based on AuNR decorated GO sheets. The high-quality of AuNR-GO nanocomposite was synthesized via the electrostatic self-assembly technique. The analytical performance of the DNA biosensor was investigated using DPV and the reduction peak current of methylene blue (MB) increased gradually with the increase of the concentration of complementary DNA. AuNRs -GO electrode exhibited the peak currents of methylene blue were linear with the logarithm of the concentrations of complementary DNA from 1.0×10^{-9} to 1.0×10^{-14} M with a detection limit of 3.5×10^{-15} M (S/*N* = 3). Moreover, the prepared electrochemical sensor could effectively distinguish complementary DNA sequences in the presence of a large amount of single-base mismatched DNA (1000:1), indicating that the biosensor has high selectivity. The biosensor showed excellent reproducibility from the results measured by fabricating five different independent electrodes. The stability of the biosensor was also investigated by detecting 1.0×10^{-11} M complementary DNA (measured everyday). It was observed no obviously changes (a ~ e) within one week. The relative standard deviation (RSD) was 0.39% ~ 0.73%, showed indicating that the DNA biosensor possesses good stability. Huang et al. [82] prepared an ultrasensitive electrochemical DNA biosensor for specific detection of human papillomavirus (HPV) DNA based on G/AuNR/PT composites. A capture probe was immobilized on a GC electrode modified with graphene/Au nanorod/polythionine (G/AuNR/PT) (Fig. 10a). Two auxiliary probes were designed and used to long-range self-assemble DNA nanostructure. The target DNA can connect DNA structure to the capture probe on the electrode surface (Fig. 10b). $[Ru(phen)_3]^{2+}$ was selected as a

Table 4 Summary of analytical performance of some gold nanorods based Enzymatic Electrochemical Sensor for the detection of small molecules

Electrode material	Fabrication method	Analyte	Detection method	Linear range	Limit of Detection	Interference	Ref.
HRP/PTMSPA@ AuNRs	simultaneously immobilizing HRP and PTMSPA on AuNRs	H_2O_2	CV, CA	1 × 10–5 to 1 × 10 − 3 M	0.06 μM (S/*N* = 3).	DA, AA, Glu	[76]
Hetero-Au@Ag NRs	multistep seed-mediated growth	Glu	CV, CA	5 μM to 10 mM	1.5 μM	DA, AA, UA	[77]
MWCNTs/GOx/ AuNR/gold	silver ion-assisted seed-mediated method	Glu	CV, CA	0.28 to 5.88 mmol L^{-1}	2.06×10^{-5} mol L^{-1}	----------	[78]
CH- prGO-AuNRs	seed-mediated growth method	Glu	CV, CA	25–200 mg.dL^{-1}	14.5 mg.dL^{-1}	Glu, Cholesterol, Urea, UA, AA	[79]

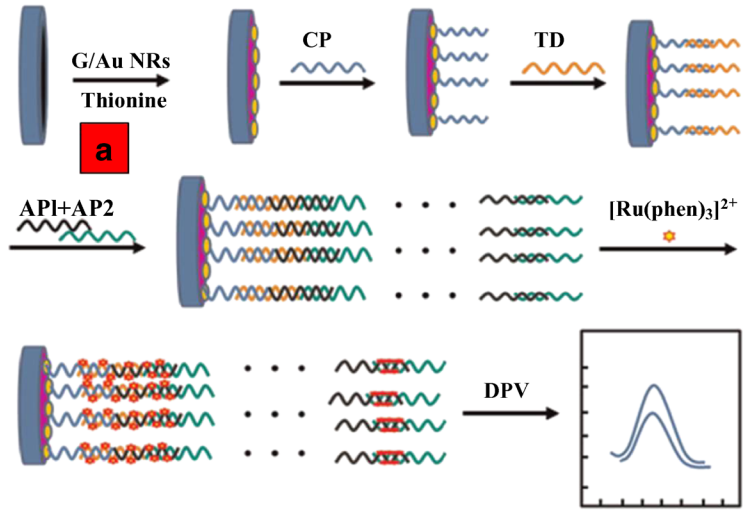

Oligonucleotide	Sequence (from 5' to 3')
capture probe (CP)	TTTCAATTTTTGGATTAC-$(CH_2)_6$-SH
complementary target DNA (TD)	GTAATCCAAAAATTGAAAACTAAGGGTCTGAGGG
auxiliary probe 1 (AP1)	TACTCCCCCAGGTGC CCCTCAGACCCTTAGT
auxiliary probe 2 (AP2)	GCACCTGGGGGAGTA ACTAAGGGTCTGAGGG
single-base mismatch target (1MT)	GTAATCCAATAATTGAAAACTAAGGGTCTGAGGG
two-base mismatch target (2MT)	GTAATCCAATTATTGAAAACTAAGGGTCTGAGGG
noncomplementary sequence (NC)	CCTTTTAGTCAGTGTGGAAATCTCTAGCAGTGGC

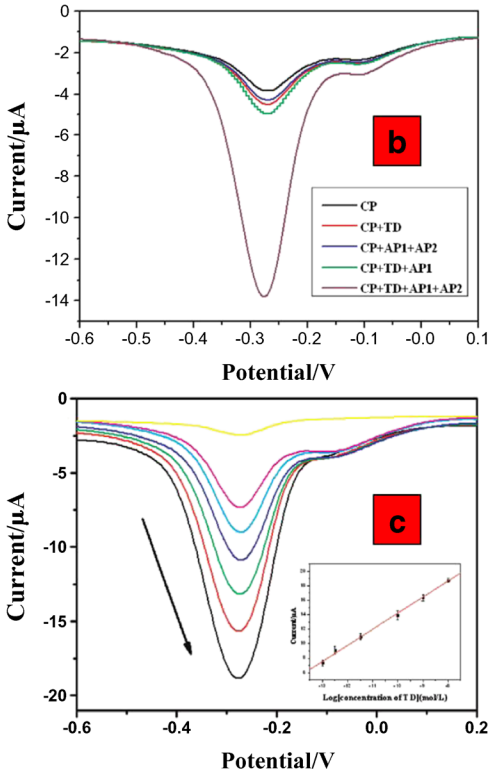

Fig. 10 **a** Schematic representation of the long-range self-assembled DNA electrochemical biosensor; Fig. 10 (**b**) DPV response of GCE modified with various oligonucleotides. The concentration of TD is 1.0×10^{-10} mol/L and the concentration of AP1 and AP2 are both 1.0×10^{-6} mol/L; Fig. 10 (**c**) DPV responses for different concentrations of TD (1.0×10^{-13}, 3.0×10^{-13}, 3.0×10^{-12}, 1.0×10^{-10}, 1.0×10^{-9} and 1.0×10^{-8} mol/L) [82]

redox indicator for amplifying electrochemical signal significantly. Enhanced sensitivity was measured through combining the excellent electric conductivity of G/AuNR/PT architecture and the long-range self-assembly DNA nanostructure with the multi-signal amplification. The DPV peak current increased with increasing the concentration of TD and a good linear relationship was observed between the peak current (i_p, A) and the logarithm of T D concentration (C, mol.L^{-1}) over the range from1.0×10^{-8} to 1.0×10^{-13} mol.L^{-1} (Fig. 9c). The detection limit was evaluated to be 4.03×10^{-14} mol.L^{-1} based on three signal-to-noise ratio. In order to investigate the selectivity of the biosensor, four kinds of DNA sequences were chosen to compare, including TD, single-base mismatch target (1MT), two-base mismatch target (2MT), and noncomplementary sequence (NC). The sensor electrode was further used for real sample analysis in human serum TD was detected in human serum in order to evaluate the performance of the method in complex condition. The DPV signal was decreased a little in complex serum sample due to the interference of the sample matrix during the hybridization between TD and CP. However, DPV response of the blank was higher in the serum than in H-buffer, which meant that the existence of the nonspecific adsorption from the components in biological sample. The results indicated the feasibility of the prepared biosensor in real physiological media.

Zimzadeh et al. [83] demonstrated a novel electrochemical nanobiosensor for plasma micro R-155 detection, based on thiolated probe-functionalized AuNRs decorated on the GO sheet on the surface of the GCE. Fig.11 shows the assembling and working procedure of the proposed electrochemical nanobiosensor for microR-155 detection. The reduction signals of a novel intercalating label Oracet Blue (OB), were 8 measured by DPV method. The electrochemical 12 signal had a linear relationship with the concentration ranging from 2.0 f. to 13 8.0 pM, and the detection limit was 0.6 fM. Furthermore, the nanobiosensor showed high Specificity, and was able to discriminate sharply between complementary target microRNA, single, three-base mismatch, and non-complementary miRNA. Alongside the outstanding sensitivity and selectivity, this nanobiosensor had great storage ability, reproducibility, and showed a decent response in the real sample analysis with plasma. Due to important role of the early and precise breast cancer detection in cancer therapy, the nano biosensor was designed for microRNA quantification, as cancer biomarkers in the plasma. Therefore, plasma was used instead of the hybridization buffer to make desired concentrations of target microR-155 (2.0, 20.0and 200.0 fM). To isolate the plasma, the blood was taken from a healthy non- cancerous people and collected in a tube containing EDTA (0.01% *v*/v of 0.5 M Na_2 EDTA (pH 8.0)) to a final concentration of 10 mM and gently

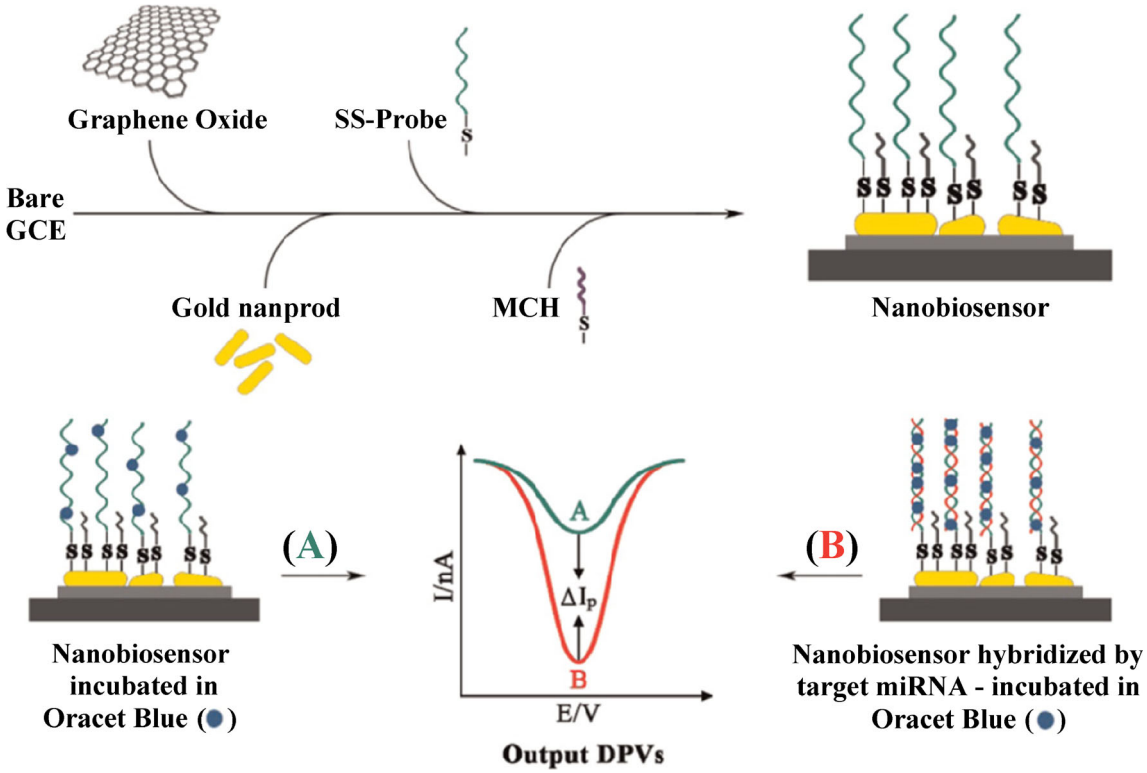

Fig. 11 Illustration of the assembling and working procedure of the proposed electrochemical nanobiosensor for miR-155 detection [83]

inverted several times. Then, the samples were centrifuged twice at 150 g for 5 min and then 350 g for 15 min and the expressed plasma were collected in a different tubes and kept isolated and frozen at −20 °C until use. The primary concentration of the miR-155 in the freshly collected plasma samples were as summed zero, because its concentration in plasma of non-cancerous people expected to be almost zero and also is lower than the detection limit of the proposed nano biosensor. Table 5 shows the summary of analytical performance of some nanorod based DNA biosensors.

Gold nanorod based Immunosensors

The early detection of cancer is of great importance for the successful treatment of disease. The tumor marker is valuable in the reflection of cell differentiation, histogenesis and cell function. In the early detection of cancer, distinguishing the malignant condition from the carcinoid condition, measuring the level of disease and finding the recurrence, tumor marker detection acts a main role. A biomarker as defined by the National Center Institute, which is a biomolecules observed in human serum and tissue that is an indicator of a biological state or a condition. The concentration of tumor marker in cancer patients significantly exceeds that of the normal adults. Various methods have been made for the detection of tumor marker such as surface Plasmon resonance immunoassay, enzyme-linked immunosorbent assay, fluorescence immunoassay, chemiluminescence immunoassay, colorimetric immunoassay and electrochemiluminescence immunoassay and electrochemical immunoassay particularly for amperometric immunosensors. Among them, amperometric immunosensors

Table 5 Summary of analytical performance of some Au nanorods based DNA Biosensors

Electrode	Fabrication method	Analyte	Detection method	Linear range	Limit of Detection	Ref.
AuNRs-GO	electrostatic self-assembly	DNA	DPV	1.0×10^{-9} to 1.0×10^{-14} M	3.5×10^{-15} M	[81]
G/AuNRs/PT	long-range self-assembled	HPV DNA	EIS, DPV	1×10^{-8} – 10 nmol/L	4.03×10^{-5} nmol/L	[82]
functionalized gold nanorods decorated on the graphene oxide (GO)	seed-mediated growth method	plasma miR-155	CV, DPV	2 f. - 8 pM	0.6 fM	[83]

attracts great attention owing to its cost effectiveness, sensitivity and simplicity [84–86].

Sun et al. [87] reported a sensitive electrochemical immunosensor for the detection of protein biomarker tumor necrosis factor α (TNF-α) that uses ferrocene carboxylic acid (Fc) functionalized self-assembled peptide nanowires (Fc-PNW) as sensor platform and glucose oxidase (GOx) modified AuNRs as label. Enhanced sensitivity was achieved based on a dual signal amplification strategy: first, the synthesized Fc-PNW used as the sensor plat form increased the loading of primary anti-TNF-α antibody (Ab_1) onto electrode surface due to its large surface area. At the same time, the Fc moiety on the nanowires is used as a mediator for GOx to catalyze the glucose reaction. Second, multiple GOx and secondary anti-TNF-α antibody (Ab_2) molecules are bounded on to each AuNR to increase the sensitivity of the immunosensor. After the preparation of the immunosensor based on the traditional sandwich protocol, the response of the immunosensor towards glucose was used as a signal to differentiate various concentrations of TNF-α. The resulting immunosensor has high sensitivity, wide linear range (0.005–10 $ng.mL^{-1}$) and good selectivity. The response of the immunosensor in phosphate buffer solution to 5 mM glucose for the detection of 10 $ng.mL^{-1}$ of TNF-α. After the addition of glucose, it can be seen that there is an increase of the oxidation current and as ignificant decrease of the reduction current, displaying a typical phenomena of GOx catalyzed glucose oxidation reaction. The high sensitivity of the immunosensor can be ascribed to the high loading ofAb_1 on the electrode surfaceand the large amount of GOx as well as Ab_2 molecules on the AuNR surface. This result indicated the successful detection of TNFα using the prepared immunosensor. The reproducibility of the immunosensor was tested since it is very important for the real application of the sensors. Six different immunosensors were prepared independently and tested for the detection of the same concentration of TNF-α. The relative standard deviations (RSD) of 5.4% and 6.1% were found for the detection of 0.1 $ng.mL^{-1}$ and 10 $ng.mL^{-1}$ of TNF-α, respectively, indicating there liability of the measurement. To demonstrate the possibility of the immunosensor for clinical applications, a recovery test was performed in human serum. The percent of TNF-α detected by the immunoasnesor from these serum samples ranged from 95.6% to 106.0% of the TNF-α added to the samples demonstrating the potential clinical applicability of the prepared immunosensor for the detection of TNF-α.

Zang et al. [88] fabricated an electrochemical immunosensor, basing on a dual signal amplified strategy by employing a biocompatible polypyrrole film-Au nanocluster matrix as a sensor platform and multi-enzyme-antibody functionalized AuNRs as an electrochemical detection label, is established for sensitive detection of ofloxacin (OFL). Finally, based on a competitive immunoassay, i.e., the association ability with the corresponding antibody between the captured antigen and free OFL in the solution, the fabricated immunosensor exhibited a sensitive response to OFL in the range from 0.08 to 410 $ng.mL^{-1}$ with a detection limit of 0.03 $ng.mL^{-1}$. The current immunosensor exhibited good sensitivity, selectivity and long-term stability. The reproducibility of the immunosensor was an important parameter for practical application. In this study, it was confirmed by three measurements of every concentration, which resulted in the relative standard deviations of 0.89%, 1.28% and 1.31% at OFL concentrations of 0.4, 6.4 and 102.4 $ng.mL^{-1}$, respectively. When the biosensor was not in use, it was stored in refrigerator at 4 °C. After 3 weeks, the catalytic current of the immunosensor decreased to about 86% of its original value, indicating the retention of the specific binding ability of the antigens. In order to evaluate the feasibility of the immunosensor for possible application, the prepared immunosensor was used to determine the recoveries of different concentrations of OFL in 0.01 M PBST buffer as a sample. A total of four PBST samples were analyzed with OFL concentrations at 0.8, 12.8, 51.2, and 204.8 $ng.mL^{-1}$, respectively. The recoveries of immunosensor ranged from 96.1 to 103.4%, indicated an acceptable accuracy. G. Sun et al. [89] constructed an ultrasensitive enzyme-free electrochemical immunosensor using AuNRs modified paper electrode as sensor platform and porous zinc oxide spheres (PZS)-silver nanoparticles (AgNPs) nanocomposites as signal labels (Fig. 12). The immunosensor for prostate specific antigen (PSA) exhibited a wide linear detection range from 0.004 to 60 $ng.mL^{-1}$ with a detection limit of 1.5 $pg.mL^{-1}$. Moreover, the immunosensor showed excellent selectivity, high stability, and acceptable fabrication reproducibility. The designed immunosensing assay results of human serum samples (provided by Shandong Cancer Hospital) were compared with the reference values (the results were provided by Shandong Tumor Hospital, China) observed by commercial available Electrochemiluminescent Analyzer (ROCHE E601, Switzerland). The immunosensor constructed in this work could be reasonably applied in the clinical determination of PSA in human plasma.

Du et al. [90] reported multi-enzyme amplification strategy using AuNRs as nanocarrier for coimmobilization of horseradish peroxidase (HRP) and detection antibody (Ab_2) at a high ratio of HRP/Ab_2, which produced an amplified electrocatalytic response by the reduction of HRP oxidized thionine in the presence of H_2O_2. Fig. 13. shows the schematic illustration of multiplexed electrochemical immunoassay. The immunoreaction processes were accelerated by applying +0.4 V for 3 min and then −0.2 V for 1.5 min; thus, the whole sandwich immunoreactions can be completed in less than 5 min. Under optimal conditions, this method could simultaneously detect phospho-$p53^{392}$, phospho-$p53^{15}$, phospho-$p53^{46}$, and

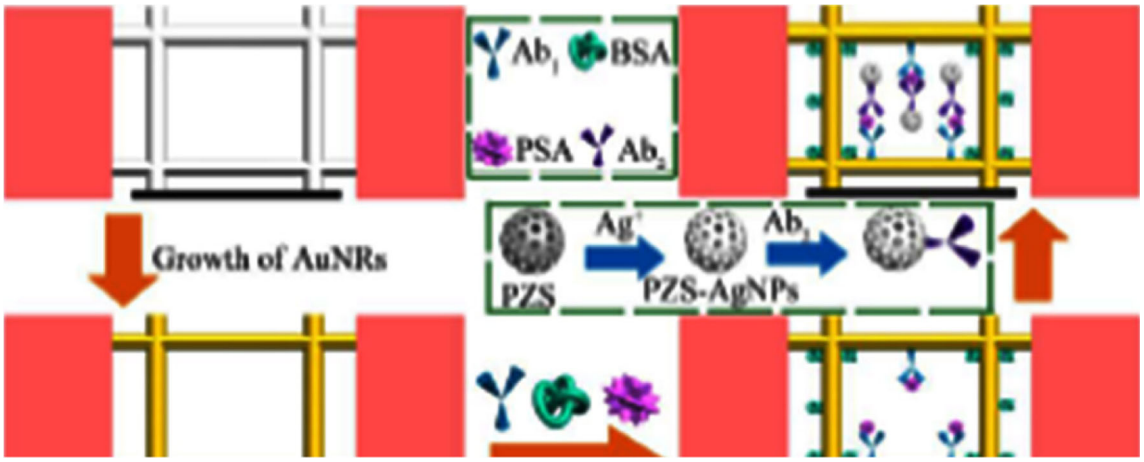

Fig. 12 The fabrication process of the AuNR-based electrochemical immunosensor [89]

total p^{53} ranging from 0.01 to 20 nM, 0.05 to 20 nM, 0.1 to 50 nM, and 0.05 to 20 nM with detection limits of 5, 20, 30, and 10 pM, respectively. Accurate determinations of these proteins in human plasma samples were demonstrated by comparison to the standard ELISA method. The disposable immunosensor array showed excellent promise for clinical screening of phosphorylated proteins and convenient point-of-care diagnostics. Table 6 depicts the summary of analytical performance of some Au nanorods Based immunosensors for the detection of small biomolecules.

Aptamer-based assays

The development of aptamer-based electrochemical biosensors as an interesting and promising technology has made the determination of small and macromolecular analytes easier, faster, and more suited for the determination of protein biomarkers. Aptamers are single stranded DNA or RNA oligonucleotides that have undergone iterative rounds of in vitro selection for binding with high affinity to specific analytes of choice; a sensitive yet easy technique to utilize aptamers as

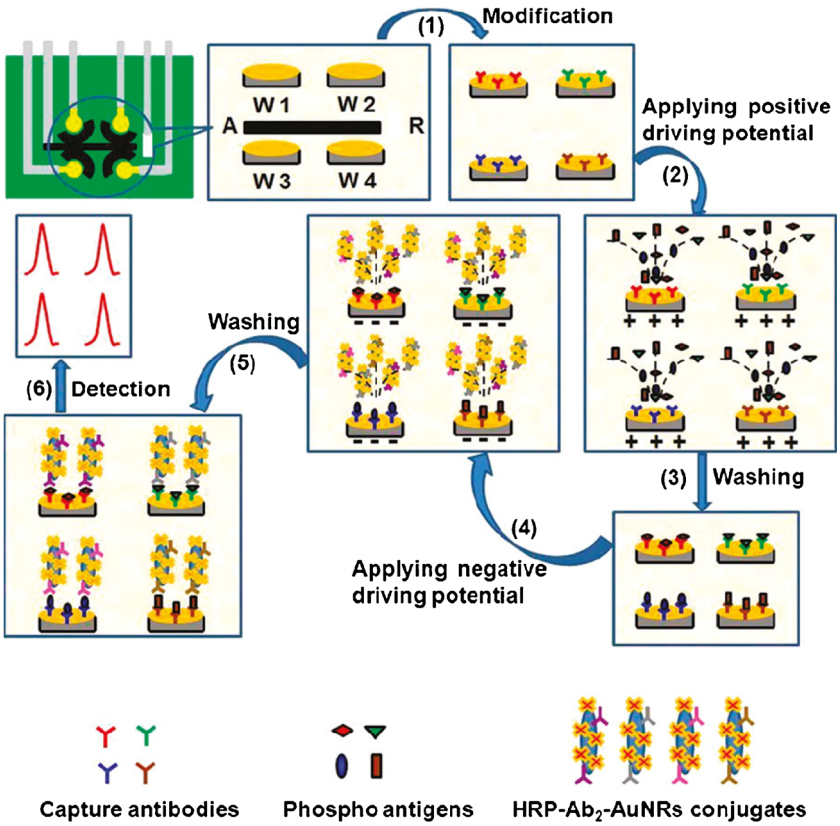

Fig. 13 Schematic illustration of multiplexed electrochemical Immunoassay by an electric field-driven process and multienzymes labeling amplification strategy using HRP-Ab2-AuNR conjugates [90]

Table 6 Summary of analytical performance of some Au nanorods Based Immunosensors for the detection of small biomolecules

Electrode material	Fabrication method	Analyte	Detection method	Linear range	Limit of detection	Ref.
glucose oxidase modified gold nanorod	seed-mediated growth method	TNF-α	CV, SWV	5 pg to 10 ng/mL	2 pg/mL based on the signal-to-noise ratio of 3.	[87]
multi-HRP- AuNR-Ab2	seed-mediated surfactant-directed approach	ofloxacin	CV	0.08 to 410 ng/mL	0.03 ng/mL	[88]
AuNR-PWE	seed-mediated growth method	prostate specific antigen	CV	0.004 to 60 ng mL^{-1}	1.5 pg mL^{-1}	[89]
HRP-Ab_2-AuNRs	Enzymelabel amplification with electric field-driven strategy	proteins	CV, SWV	0.01 to 20 nM (phospho-$p53^{392}$), 0.05 to 20 nM (phospho-$p53^{15}$), 0.1 to 50 nM (phospho-$p53^{46}$), and 0.05 to 20 nM (p^{53})	5 pM (phospho-$p53^{392}$), 20 pM (phospho-$p53^{15}$), 30 pM (phospho-$p53^{46}$), and 10 pM (p^{53})	[90]

recognition entities for the fabrication of electrochemical biosensors is to transduce the signal electrochemically [91]. Aptamers based electrochemical biosensors provide a number of advantages over conventional antibody including low cost, temperature stability and reusability [92]. Shakoori et al. [93] fabricated an electrochemical DNA biosensor based on AuNRs on a gold-electrode surface for detecting HBV. The authors studied the construction process of the biosensor using CV of $[Fe(CN)_6]^{3-/4-}$, as an electrochemical redox probe, and of $[Co(phen)3]3^{+}$, as an electrochemical indicator. The target DNA was quantified in the linear range from 1.0×10^{-12} to 10.0×10^{-6} mol.L^{-1}, with a detection limit of 2.0×10^{-12} mol.L^{-1}. The DNA biosensor exhibited good specificity for distinguishing complementary DNA from non-complementary and mismatched DNA sequences. The sequence of oligonucleotides was selected using BLAST so that it had the least similarity to the human serum genome.

W. Wen et al., [94] reported a triplex signal amplification strategy for sensitive biosensing of cancer biomarker by taking advantage of hairpin-shaped oligonucleotide-functionalized gold nanorods (HO-AuNRs), graphene and the avidin-biotin reation. Fig. 14a and b depicts the modification and assembly process of SA-CS/GR/GCE and electrochemical sensing strategy for the detection of CEA (carcinoembryonic antigen). The strategy was expanded for the electrochemical detection of carcinoembryonic antigen (CEA) by using an aptamer as biosensor's recognition element and HO-AuNRs as signal enhancer. The biosensor was constructed by the GNR was used as a carrier of horseradish peroxidase (HRP) and HO aptamer with a biotin at the 3′-end and a thiol at the 5′-end, which amplified the electrochemical response because of a large molar ratio of HRP to HO. In the presence of target CEA, the binding reactions of CEA with the loop portions of the HOs caused HOs' loop-stem structure opened and exposed the biotins and then HRP-AuNRs-HO conjugates were captured on graphene and streptavidin modified electrodes via the reaction between the exposed biotins and preimmobilized streptavidins. The accumulation of HRP effectively catalyzed the hydrogen peroxide-mediated oxidation of o-phenylenediamine to generate an electrochemical reduction current for CEA detection. Under optimal conditions, the electrochemical biosensor exhibited a wide dynamic range of 5 pg.mL^{-1} and 50 ng.mL^{-1} toward CEA standards with a low detection limit of 1.5 pg.mL^{-1} (signal-to-noise ratio ofs 3). The biosensor accurately detected CEA concentration in 8 human serum samples from patients with lung diseases, showing excellent correlations with standard chemiluminescence immunoassay.

Gallina et al. [95] used aptamer-conjugated, fluorescent AuNRs as potential cancer theradiagnostic agents. The aspect ratio of AuNRs was 3.9. Bioconjugation with a fluorescent, active targeting agent, H_2N-AS1411-Cy5, was secured using a versatile cross-linking method based on the exploitation of

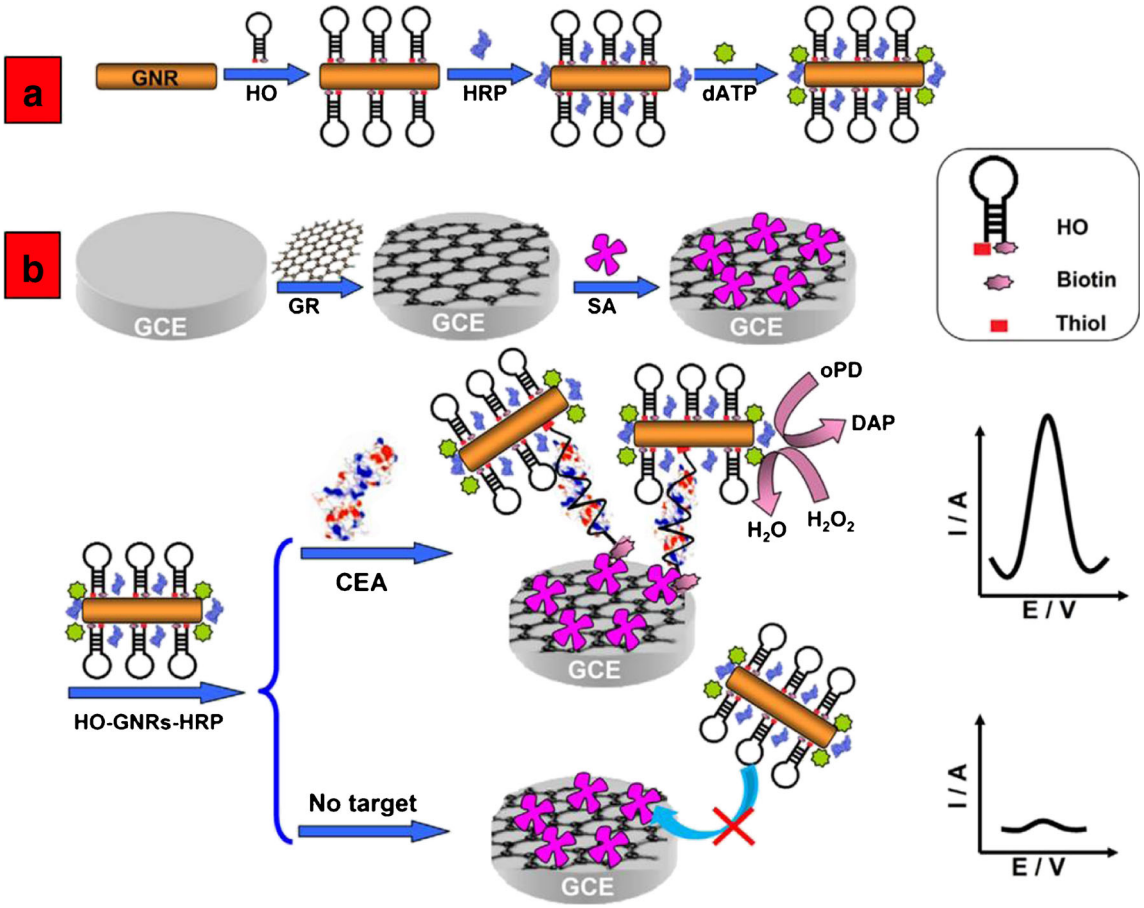

Fig. 14 **a** Modification procedure of HO- AuNRs-HRP conjugate; Fig. 14. (**b**) Schematic illustration of the assembly process of SA-CS/GR/GCE and electrochemical sensing strategy for the detection of CEA [94]

aptamers' modularity. The fluorescent version of AS1411 was internalized by cancer cells via endocytosis. Flow cytometry experiments and far-field fluorescence microscopic studies evidenced the efficiency of AC-GNR uptake by cancer cells. The authors also found that AC-GNRs were good candidates for theradiagnostic applications based on the use of photothermal therapy.

Conclusion and future outlooks

To determine the very low level of biomoleclues and identify early stages of diseases extremely sensitive biosensors are needed. An electrochemical sensor is one of the best candidates having rapid, high sensitive and selective determination of analytes. In this review article, we have described the synthesis of gold nanorods by various techniques such as electrochemical synthesis, seed-mediated synthesis, template method, lithographic methods and catalytic methods have been discussed. The importance of electrochemistry of AuNRs was also addressed. The AuNR nanoelectrodes offer great opportunities to do electrochemistry in highly sensitive and to examine the kinetics of redox procedures that are too fast to assess at conventional macroscopic electrodes. We have highlighted the use AuNR-based non-enzymatic electrochemical sensor for simple biomolecules including hydrogen peroxide, nitric oxide, glucose, dopamine, NAD^+ and NADH, L-Cysteine and other analytes have been discussed. Besides, AuNR-based enzymatic electrochemical sensor for simple biomolecules and AuNR-based DNA biosensors, immunosensors and biomarkers were discussed. In conclusion, the AuNRs-based materials and its unique electronic properties make outstanding sensing material in the development of electrochemical biosensor. However, the AuNR based electrochemical biosensor for the detection of important biomolecules such as NAD^+ and NADH, L-cysteine and biomarkers are rarely reported. Microfluidic paper-based analytical device with electrochemical detection (ePADs) provides a selective and sensitive platform for evaluating biomarkers in the near future. Noiphung et al. [96] reported the electrochemical detection of glucose in whole blood using reusable, external screen-printed carbon electrode modified with a mediator, Prussian Blue. Blood plasma carrying glucose was separated from whole blood into a detection region where it reacted with glucose oxidase to form hydrogen peroxide, and detected electrochemically using amperometry. This ePAD device was

capable of sub-nanomolar detection and offered results comparable to HPLC testing of real human samples. It was observed from the reports that the electrocatalytic activity of AuNRs not only depends on aspect ratio but also depends on the functionalization and active catalytic sites on AuNRs surface. Therefore, one can achieve a novel AuNR-based electrocatalyst for a particular electrocatalytic process by optimizing several parameters such as aspect ratio, functionalization, facet growth control, stability of the modified electrode etc. In future, paper based gold nanorods obtaining by incorporating with paper microfluidic technique, which may suitable for the electrochemical sensing of small biomolecules [97]. Hence, in future the selective and sensitive determination of those molecules has become essential for public health. In the near future, development of multi-analysis, highly specific, highly sensitive nanoscale biosensors will need the combination of interdisciplinary knowledge from various fields including surface biochemistry, medicine, biology and bioengineering, solid-state and surface physics and electrical engineering. Any development in this area will have an outcome on the future of health care and diagnostics. The AuNR-based materials and its modified electrode is a versatile system for the detection of important biomolecules in the near future.

Acknowledgments PR and AP dedicated this article to Professor R.Ramaraj, CSIR-Emeritus Scientist, School of Chemistry, Madurai Kamaraj University for his pioneer contribution in electrocatalysis and sensors.

Compliance with ethical standards The author(s) declare that they have no competing interests.

References

1. Song S, Xu H, Fan C (2006) Potential diagnostic applications of biosensors: current and future directions. Int J Nanomedicine 1(4): 433–440
2. Wang J (1999) Sol–gel materials for electrochemical biosensors. Anal Chim Acta 399(1):21–27
3. Singh P, Pandey SK, Singh J, Srivastava S, Sachan S, Singh SK (2016) Biomedical perspective of electrochemical Nanobiosensor. Nano-Micro Lett 8(3):193–203
4. Jayabal S, Pandikumar A, Lim HN, Ramaraj R, Sun T, Huang NM (2015) A gold Nanorods-based localized surface Plasmon resonance platform for the detection of environmentally toxic metal ions. Analyst 140:2540–2555
5. Prasad BB, Singh R, Kumar A (2016) Gold nanorods *vs.* gold nanoparticles: application in electrochemical sensing of cytosine β-D-arabinoside using metal ion mediated molecularly imprinted polymer. RSC Adv 6:80679–80691
6. Huang XH, Neretina S, El-Sayed MA (2009) Gold nanorods: from synthesis and properties to biological and biomedical applications. Adv Mater 21:4880–4910
7. Narayanan R, El-Sayed MA (2005) Catalysis with transition metal nanoparticles in colloidal solution: nanoparticle shape dependence and stability. J Phys Chem C 109:12663–12676
8. Haberlen OD, Chung SC, Stener M, Rosch N (1997) From clusters to bulk: A relativistic density functional investigation on a series of gold clusters Au_n, n=6,…,147. J Chem Phys 106:5189
9. Sau TK, Rogach AL, Jackel F, Klar TA, Feldmann J (2010) Properties and applications of colloidal nonspherical noble metal nanoparticles. Adv Mater 22:1805–1825
10. Bastus NG, Comenge J, Puntes V (2011) Kinetically controlled seeded growth synthesis of citrate-stabilized gold nanoparticles of up to 200 nm: size focusing versus Ostwald ripening. Langmuir 27: 11098–11105
11. Wu H-Y, Chu H-C, Kuo T-J, Kuo C-L, Huang MH (2005) Seed-mediated synthesis of high aspect ratio gold Nanorods with nitric acid. Chem Mater 17:6447–6451
12. Jia H, Fang C, Zhu X-M, Ruan Q, Wang Y-X J, Wang J (2015) Synthesis of absorption-dominant small gold Nanorods and their Plasmonic properties. Langmuir 31:7418–7426
13. Pontifex GH, Zhang P, Wang Z, Haslett TL, AlMawlawi D, Moskovits M (1991) STM imaging of the surface of small metal particles formed in anodic oxide pores. J Phys Chem 95:9989–9993
14. Gole A, Murphy CJ (2004) Seed-mediated synthesis of gold Nanorods: role of the size and nature of the seed. Chem Mater 16:3633–3640
15. Nikoobakht B, El-Sayed MA (2003) Preparation and growth mechanism of gold Nanorods (NRs) using seed-mediated growth method. Chem Mater 15:1957–1962
16. Lamprect G, Pichlmayer F, Schmid ER (1994) Determination of the authenticity of vanilla extracts by stable isotope ratio analysis and component analysis by HPLC. J Agric Food Chem 42:1722–1727
17. Ni Y, Zhang G, Kokot S (2005) Simultaneous spectrophotometric determination of maltol, ethyl maltol, vanillin and ethyl vanillin in foods by multivariate calibration and artificial neural networks. Food Chem 89:465–473
18. Boyce MC, Haddad PR, Sostaric T (2003) Determination of flavour components in natural vanilla extracts and synthetic flavourings by mixed micellar electrokinetic capillary chromatography. Anal Chim Acta 485:179–186
19. Sostaric T, Boyce MC, Spickett EE (2000) Analysis of the volatile components in vanilla extracts and flavorings by solid-phase microextraction and gas chromatography. J Agric Food Chem 48: 5802–5807
20. Peng H, Wang S, Zhang Z, Xiong H, Li J, Chen L, Li Y (2012) Molecularly imprinted photonic hydrogels as colorimetric sensors for rapid and label-free detection of vanillin. J Agric Food Chem 60: 1921–1928
21. Yusoff N, Pandikumar A, Ramaraj R, Huang NM, Lim HN (2015) Gold nanoparticles based optical and electrochemical sensing of dopamine. Microchim Acta 182:2091–2114
22. Pandikumar A, How GTS, Teo PS, Fatin SO, Jayabal S, Kamali KZ, Yusoff N, Asilah J, Ramaraj R, Abraham John S, Lim HN, Huang NM (2014) Graphene and its nanocomposite material based electrochemical sensor platform for dopamine. RSC Adv 4:63296–63323
23. Pandikumar A, How GTS, See TP, Omar FS, Jayabal S, Kamali KZ, Yusoff N, Jamil A, Ramaraj R, John SA, Limbe HN, Huang NM (2014) Graphene and its nanocomposite material based electrochemical sensor platform for dopamine. RSC Adv 4:63296
24. Yu Y, Chang SS, Lee CL, Wang CRC (1997) Gold Nanorods: electrochemical synthesis and optical properties. J Phys Chem B 101:6661–6664
25. Chang SS, Shih CW, Chen CD, Lai WC, Wang CRC (1999) The shape transition of gold Nanorods. Langmuir 15:701–709
26. Vigderman L, Khanal BP, Eugene RZ (2012) Functional gold Nanorods: synthesis, self-assembly, and sensing applications. Adv Mater 24:4811–4841
27. Jana NR, Gearheart L, Murphy CJ (2001) Seed-mediated growth approach for shape-controlled synthesis of spheroidal

and rod-like gold nanoparticles using a surfactant template. Adv Mater 13:1389–1393
28. Zweifel DA, Wei A (2005) Sulfide-arrested growth of gold Nanorods. Chem Mater 17:4256–4261
29. Dickson W, Evans PR, Wurtz GA, Hendren W, Atkinson R, Pollard RJ, Zayatz AV (2008) Towards nonlinear plasmonic devices based on metallic nanorods. J Microsc 229:415–420
30. Van der Zande BMI, MBoehmer R, Fokkink LGJ, Schoenenberger C (2000) Colloidal dispersions of gold rods: synthesis and optical properties. Langmuir 16:451–458
31. Grand J, Kostcheev S, Bijeon JL, de la Chapelle ML, Adam PM, Rumyantseva A, Lerondel G, Royer P (2003) Optimization of SERS-active substrates for near-field Raman spectroscopy. Synth Met 139:621
32. Cubukcu E, Kort EA, Crozier KB, Capasso F (2006) Plasmonic laser antenna. Appl Phys Lett 89:093120
33. Taub N, Krichevski O, Markovich G (2003) Growth of gold Nanorods on surfaces. J Phys Chem B 107:11579–11582
34. Wei Z, Mieszawska AJ, Zamborini FP (2004) Synthesis and manipulation of high aspect ratio gold Nanorods grown directly on surfaces. Langmuir 20:4322
35. Liao H, Hafner JH (2004) Monitoring gold Nanorod synthesis on surfaces. J Phys Chem B 108:19276–19280
36. Shopova SI, Blackledge CW, Rosenberg AT (2006) Gold nanorods grown from HgTe nanoparticles directly on various surfaces. Appl Phys Lett 89:023120
37. Mieszawska AJ, Zamborini FP (2005) Gold Nanorods grown directly on surfaces from microscale patterns of gold seeds. Chem Mater 17:3415–3420
38. Xia H, Li L, Yin Z, Hou X, Zhu JJ (2015) Biobar-coded gold nanoparticles and DNAzyme-based dual signal amplification strategy for ultrasensitive detection of protein by Electrochemiluminescence. ACS Appl Mater Interfaces 7:696–703
39. Liu J, He X, Wang K, He D, Wang Y, Mao Y, Shi H, Wen L (2015) A highly sensitive electrochemiluminescence assay for protein kinase based on double-quenching of graphene quantum dots by G-quadruplex–hemin and gold nanoparticles. Biosens Bioelectron 70: 54–60
40. Chirea M, Cruz A, Pereira CM, Silva AF (2009) Size-dependent electrochemical properties of gold Nanorods. J Phys Chem C 113: 13077–13087
41. Chirea M, Garcia-Morales V, Manzanares JA, Pereira C, Gulaboski R, Silva FJ (2005) Electrochemical characterization of polyelectrolyte/gold nanoparticle multilayers self-assembled on gold electrodes. Phys Chem B 109:21808–21817
42. Chirea M, Pereira CM, Silva F (2007) Catalytic effect of gold nanoparticles self-assembled in multilayered polyelectrolyte films. J Phys Chem C 111:9255–9266
43. Chirea M, Borges J, Pereira CM, Silva AF (2010) Density-dependent electrochemical properties of vertically aligned gold Nanorods. J Phys Chem C 114:9478–9488
44. Gooding JJ, Chou A, Liu JQ, Losic D, Shapter JG, Hibbert DB (2007) The effects of the lengths and orientations of single-walled carbon nanotubes on the electrochemistry of nanotube-modified electrodes. Electrochem Commun 9:1677–1683
45. Chidsey CED (1991) Free energy and temperature dependence of electron transfer at the metal-electrolyte Interface. Science 251: 919–922
46. Lin CC, Juo TJ, Chen YJ, Chiou CH, Wang HW, Liu YL (2008) Enhanced cyclic voltammetry using 1-D gold nanorods synthesized via AAO template electrochemical deposition. Desalination 233: 113–119
47. Munshi AM, Ho D, Saunders M, Agarwal V, Raston CL, Iyer KS (2016) Influence of aspect ratio of magnetite coated gold nanorods in hydrogen peroxide sensing. Sensors Actuators B Chem 235:492–497
48. Jayabal S, Ramaraj R (2013) Synthesis of core/shell au/ag nanorods embedded in functionalized silicate sol–gel matrix and their applications in electrochemical sensors. Electrochim Acta 88:51–58
49. Xun F, Hongyan XL, Hao S, Xiaochun H, Song WW (2014) Highly accessible Pt nanodots homogeneously decorated on au nanorods surface for sensing. Anal Chim Acta 852:37–44
50. Pang P, Yang Z, Xiao S, Xie J, Zhang Y, Gao Y (2014) Nonenzymatic amperometric determination of hydrogen peroxide by graphene and gold nanorods nanocomposite modified electrode. J Electroanal Chem 727:27–33
51. Wang C, Zou X, Wang Q, Shi K, Tan J, Zhao X, Chaia Y, Yuan R (2014) A nitrite and hydrogen peroxide sensor based on Hb adsorbed on au nanorods and graphene oxide coated by polydopamine. Anal Methods 6:758
52. Yang X, Wang Y, Liu Y, Jiang X (2013) A sensitive hydrogen peroxide and glucose biosensor based on gold/silver core–shell nanorods. Electrochim Acta 108:39–44
53. Dang X, Hu H, Wang S, Hu S (2015) Nanomaterial-based electrochemical sensors for nitric oxide. Microchim Acta 182:455–467
54. Vasilescu A, Gheorghiu M, Peteu S (2017) Nanomaterial-based electrochemical sensors and optical probes for detection and imaging of peroxynitrite: a review. Microchim Acta 184:649–676
55. Jayabal S, Viswanathan P, Ramaraj R (2014) Reduced graphene oxide–gold nanorods composite material stabilized in silicate sol–gel matrix for nitric oxide sensor. RSC Adv 4:33541
56. Marlinda AR, Pandikumar A, Jayabal S, Yusoff N, Suriani AB, Huang NM (2016) Voltammetric determination of nitric oxide using a glassy carbon electrode modified with a nanohybrid consisting of myoglobin, gold nanorods, and reduced graphene oxide. Microchim Acta 183:3077–3085
57. Zhao Y, Fang X, Yan X, Zhang X, Kang Z, Zhang G, Zhang Y (2015) Nanorod arrays composed of zinc oxide modified with gold nanoparticles and glucose oxidase for enzymatic sensing of glucose. Microchim Acta 182(3–4): 605–610
58. Zhang C, Ni H, Chen R, Zhan W, Zhang B, Lei R, Zha Y (2015) Enzyme-free glucose sensing based on Fe3O4 nanorod arrays. Microchim Acta 182(9–10):1811–1818
59. Tamer U, Seckin AI, Temur E, Torul H (2011) Fabrication of biosensor based on polyaniline/gold Nanorod composite. Int J Electrochem 2011:7
60. Yingying L, Xiaoxia W, Xiang D, Zhipeng H, Haiqian Z (2010) Amperometric glucose biosensor based on gold nanorods and chitosan comodified au electrode. Rare Metals 29:238–242
61. Ciftci H, Tamer U (2012) Functional gold nanorod particles on conducting polymer poly(3-octylthiophene) as non-enzymatic glucose sensor. React Funct Polym 72:127–132
62. Ren X, Chen D, Meng X, Tang F, Du A, Zhang L (2009) Amperometric glucose biosensor based on a gold nanorods/cellulose acetate composite film as immobilization matrix. Colloids Surf B 72:188–192
63. Hsu CW, JenWang G (2014) Highly sensitive glucose biosensor based on au–Ni coaxial nanorod array having high aspect ratio. Biosens Bioelectron 56:204–209
64. Liu H, Chen D, Yang L, Ren X, Tang F, Ren J (2010) A study of the electron transfer and photothermal effect of gold nanorods on a glucose biosensor. Nanotechnology 21:185504
65. Ahn M, Kim J (2012) Electrochemical behavior of dopamine and ascorbic acid at dendritic au rod surfaces: selective detection of dopamine in the presence of high concentration of ascorbic acid. J Electroanal Chem 683:75–79
66. Deng C, Chen J, Yang M, Nie Z, Si S (2011) Electrochemical determination of dopamine in the presence of ascorbic acid based on the gold nanorods/carbon nanotubes composite film. Electrochim Acta 56:8851–8856

67. Jia Z, Liu J, Shen Y (2007) Fabrication of a template-synthesized gold nanorod-modified electrode for the detection of dopamine in the presence of ascorbic acid. Electrochem Commun 9:2739–2743
68. Li L, Lu H, Deng L (2013) A sensitive NADH and ethanol biosensor based on graphene-au nanorods nanocomposites. Talanta 113: 1–6
69. Jayabal S, Ramaraj R (2015) Amperometric sensing of NADH at gold nanorods stabilized in amine-functionalized silicate sol–gel matrix modified electrode. J Appl Electrochem 45:881–888
70. Silva FDADS, Silva MGAD, Lima PR, Meneghetti MR, Kubota LT, Goulart MOF (2013) A very low potential electrochemical detection of L-cysteine based on a glassy carbon electrode modified with multi-walled carbon nanotubes/gold nanorods. Biosens Bioelectron 50:202–209
71. Jagriti N, Nitesh M, Gajendra S, Pundir CS (2015) Electrochemical impediometric detection of anti-HIV drug taking gold nanorods as a sensing interface. Biosens Bioelectron 66:332–337
72. Bai W, Huang H, Li Y, Zhang H, Liang B, Guo R, Du L, Zhang Z (2014) Direct preparation of well-dispersed graphene/gold nanorodcomposites and their application in electrochemical sensors for determination of ractopamine. Electrochim Acta 117:322–328
73. Rahi A, Sattarahmady N, Vais RD, Heli H (2015) Sonoelectrodeposition of gold nanorods at a gold surface – Applicationfor electrocatalytic reduction and determination of nitrofurazone. Sensors Actuators B Chem 210:96–102
74. Mengdong W, Yitao H, Xingxing L, Zhou N, Chunyan D, Manli G, Shouzhuo Y (2011) Assembly of layer-by-layer films of superoxide dismutase and gold nanorods: a third generation biosensor for superoxide anion. Sci China Mater 54:1284–1291
75. Arvand M, Gholizadeh TM (2013) Gold nanorods-graphene oxide nanocomposite incorporated carbonnanotube paste modified glassy carbon electrode for voltammetric determination of indomethacin. Sensors Actuators B Chem 186:622–632
76. Komathi S, Gopalan AI, Kim SK, Anand GS, Lee KP (2013) Fabrication of horseradish peroxidase immobilized poly(N-[3-(trimethoxy silyl)propyl]aniline) gold nanorods film modified electrode and electrochemical hydrogen peroxide sensing. Electrochim Acta 92:71–78
77. Zhang S, Han L, Hou C, Li C, Lang Q, Han L, Liu A (2015) Novel glucose sensor with au@ag heterogeneous nanorods based on electrocatalytic reduction of hydrogen peroxide at negative potential and neutral pH. J Electroanal Chem 742:84–89
78. Li Y, Wang F, Huang F, Li Y, Feng S (2012) Direct electrochemistry of glucose oxidase and its biosensing to glucose based on the chit-MWCNTs–AuNRs modified gold electrode. J Electroanal Chem 685:86–90
79. Nirala NR, Abraham S, Kumar V, Pandey SA, Yadav U, Srivastava M, Srivastava SK, Singh VN, Kayastha AM, Srivastava A, Saxena PS (2015) Partially reduced graphene oxide-gold nanorods composite based bioelectrode of improved sensing performance. Talanta 144:745–754
80. Rasheed PA, Sandhyarani N (2017) Electrochemical DNA sensors based on the use of gold nanoparticles: a review on recent developments. Microchim Acta 84:981–1000
81. Han X, Fang X, Shi A, Wang J, Zhang Y (2013) An electrochemical DNA biosensor based on gold nanorods decorated graphene oxide sheets for sensing platform. Anal Biochem 443:117–123
82. Huang H, Bai W, Dong C, Guo R, Liu Z (2015) An ultrasensitive electrochemical DNA biosensor based on graphene/ au nanorod/ polythionine for human papillomavirus DNA detection. Biosens Bioelectron 68:442–446
83. Azimzadeh M, Rahaiea M, Navid Nasirizadeh N, Ashtari K, Manesh HN (2016) An electrochemical nanobiosensor for plasma miRNA-155, based on graphene oxide and gold nanorod, for early detection of breast cancer. Biosens Bioelectron 77:99–106
84. Zhang Y, Ge L, Li M, Yan M, Ge S, Yu J, Song X, Cao B (2014) Flexible paper-based ZnO nanorod light-emitting diodes induced multiplexed photoelectrochemical immunoassay. Chem Commun 50:1417–1419
85. Shan J, Ma Z (2017) A review on amperometric immunoassays for tumor markers based on the use of hybrid materials consisting of conducting polymers and noble metal nanomaterials. Microchim Acta 184:969–979
86. Hasanzadeh M, Shadjou N (2017) Advanced nanomaterials for use in electrochemical and optical immunoassays for the carcinoembryonic antigen. A review. Microchim Acta 184: 389–414
87. Sun Z, Deng L, Gan H, Shen R, Yang M, Zhang Y (2013) Sensitive immunosensor for tumor necrosis factor based on dual signal amplification of ferrocene modified self-assembled peptide nanowire and glucose oxidase functionalized gold nanorods. Biosens Bioelectron 39:215–219
88. Zang S, Liu Y, Lin M, Kang J, Sun Y, Lei H (2013) A dual amplified electrochemical immunosensor for ofloxacin: Polypyrrole film-au nanocluster as the matrix and multi-enzyme-antibody functionalized gold nanorod as the label. Electrochim Acta 90:246–253
89. Sun G, Liu H, Zhang Y, Yu J, Yan M, Song X, He W (2015) Gold nanorods-paper electrode based enzyme-free electrochemical immunoassay of prostate specific antigen using porous zinc oxide spheres-silver nanoparticles nanocomposites as labels. New J Chem 39:6062–6067
90. Du D, Wang J, Lu D, Dohnalkova A, Lin Y (2011) Multiplexed electrochemical immunoassay of phosphorylated proteins based on enzyme-functionalized gold Nanorod labels and electric field-driven acceleration. Anal Chem 83:6580–6585
91. Cheng AKH, Sen D, Yu HZ (2009) Design and testing of aptamer-based electrochemical biosensors for proteins and small molecules. Bioelectrochemistry 77:1–12
92. Liu Y, Tuleouva N, Ramanculov E, Revzin A (2010) Aptamer-based electrochemical biosensor for interferon gamma detection. Anal Chem 82:8131–8136
93. Shakoori Z, Salimian S, Kharrazi S, Adabi M, Saber R (2015) Electrochemical DNA biosensor based on gold nanorods for detecting hepatitis B virus. Anal Bioanal Chem 407: 455–461
94. Wen W, Huang JY, Bao T, Zhou J, Xia HX, Zhang XH, Wang SF, Zhao YD (2016) Increased electrocatalyzed performance through hairpin oligonucleotide aptamer-functionalized gold nanorods labels and graphene-streptavidin nanomatrix: highly selective and sensitive electrochemical biosensor of carcinoembryonic antigen. Biosens Bioelectron 83:142–148
95. Gallina ME, Zhou Y, Johnson CJ, Harris-Birtill D, Singh M, Zhao H, Ma D, Cass T, Elson DS (2016) Aptamer-conjugated, fluorescent gold nanorods as potential cancer theradiagnostic agents. Mater Sci Eng C 59:324–332
96. Noiphung J, Songjaroen T, Dungchai W, Henry CS, Chailapakul O, Laiwattanapaisal W (2013) Electrochemical detection of glucose from whole blood using paper-based microfluidic devices. Anal Chim Acta 788:39–45
97. Cate DM, Adkins JA, Mettakoonpitak J, Henry CS (2015) Recent developments in paper-based microfluidic devices. Anal Chem 87(1):19–41